Accepted Manuscript

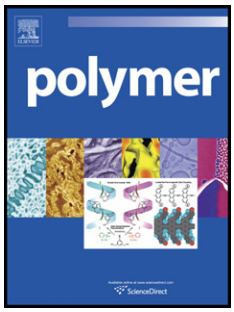

Pore formation in polystyrene fiber by superimposing temperature and relative humidity of electrospinning atmosphere

H. Fashandi, M. Karimi

PII: S0032-3861(12)00847-6

DOI: 10.1016/j.polymer.2012.10.003

Reference: JPOL 15720

To appear in: *Polymer*

Received Date: 8 April 2012

Revised Date: 14 September 2012

Accepted Date: 2 October 2012

Please cite this article as: Fashandi H, Karimi M, Pore formation in polystyrene fiber by superimposing temperature and relative humidity of electrospinning atmosphere, *Polymer* (2012), doi: 10.1016/j.polymer.2012.10.003.

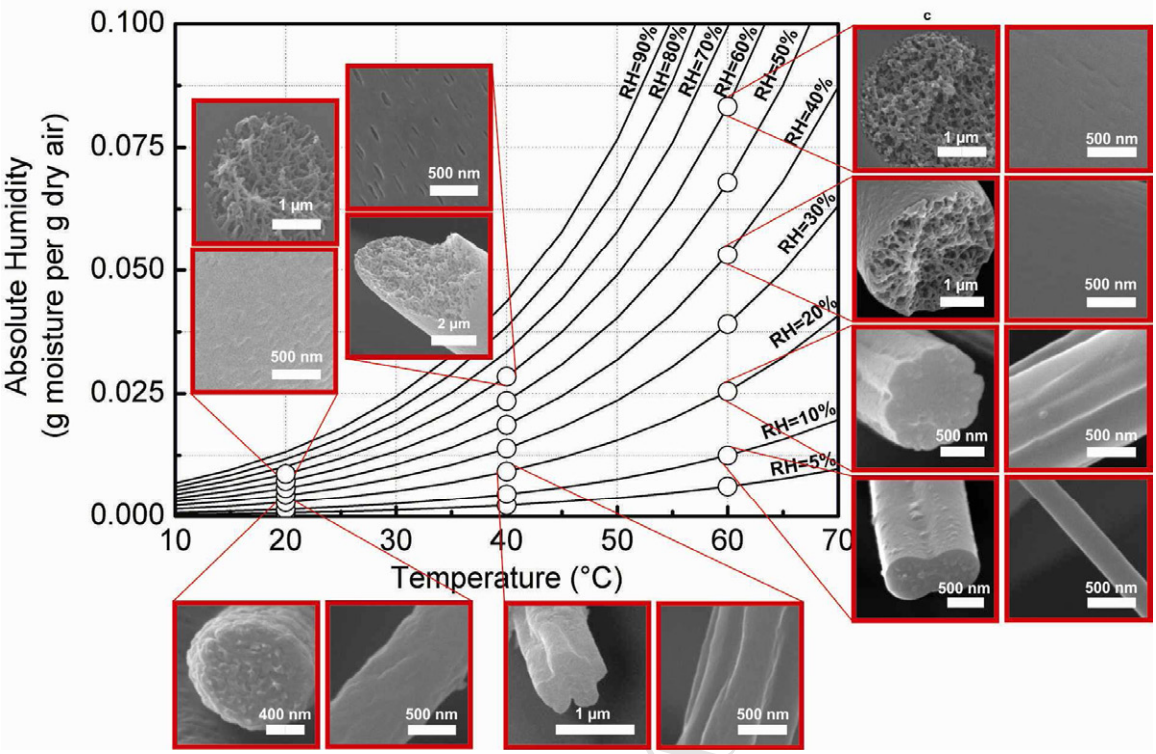

Pore formation in polystyrene fiber by superimposing temperature and relative humidity of electrospinning atmosphere

H. Fashandi, M. Karimi*

Amirkabir University of Technology, Department of Textile Engineering, Hafez Avenue, Tehran, 15914, Iran

*Tel: +98-21-6454-2600. Fax: +98-21-66400245.

E-mail: mkarimi@aut.ac.ir

Abstract

We report evolving pore formation in both surface and interior structures of polystyrene (PS) fibers electrospun from solutions of dimethylformamide (DMF), as low, and tetrahydrofuran (THF), as high volatile solvents. The environmental conditions, i.e., temperature and relative humidity of electrospinning process were systematically changed using a high-accuracy conditioning box to provide a comprehensive investigation of morphology evolution within electrospun fibers. Three angle phase diagrams of H_2O/DMF/PS and H_2O/THF/PS systems were constructed at temperature of 20, 40, and 60 ºC by measuring the cloud points as well as calculating the free energy of mixing, in order to analyze the thermodynamic instability of polymer solution jet undergoing solvent evaporation and water penetration. According to the results, pores form within the fiber if DMF has low volatility and develop onto the fiber surface if THF high volatile solvent is employed. In the former case vapor-induced phase separation is involved while in latter case mechanism of breath-figure formation is dominant. Three types of morphology for fiber surface, i.e., non-porous, porous and wrinkled are recognized as relative humidity and temperature of electrospinning process vary. Morphology transition of surface fiber is taken place at certain relative humidity while it shifts by varying the temperature. Superimposing the relative humidity and temperature not only describes the suppression of bead formation but also controls the mean diameter of electrospun fiber.

Keywords: Electrospinning, Temperature, Relative humidity, Polystyrene (PS), Nanoporous fibers, Wrinkled surface. Breath figure, Phase separation.

Abbreviation			
PS	polystyrene	VIPS	vapor-induced phase separation
DMF	N,N-dimethylformamide	SD	spinodal decomposition
THF	tetrahydrofuran	NG	nucleation & growth
DCM	dichloromethane	SEM	scanning electron microscope
VPO	vapor pressure osmometer	*FPV*	Fractional interior pore volume
Nomenclature			
T	absolute temperature (K)	u_2	volume fraction of pseudo binary mixture
T_g	Glass transition temperature (K)	π	osmotic pressure (Pa)
RH	relative humidity (%)	$\Delta\Phi_{el}$	voltage difference (V)
ω	absolute humidity	K	calibration constant
P_a	partial pressure of air (atm)	ν	molar volume ($cm^3\ mol^{-1}$)
P_g	saturation pressure of vapor in a given temperature (atm)	υ	Specific volume ($cm^3\ g^{-1}$)
φ	volume fraction	R	gas constant (8.314 J $mol^{-1}\ K^{-1}$)
ΔG_M	Gibbs free energy of mixing	ρ	density ($g\ cm^{-3}$)
V	volume (cm^3)	ρ^*	hard-core density ($g\ cm^{-3}$)
n	number of moles	α	thermal expansion coefficient (K^{-1})
N	number of molecules	x	mole fraction
χ	interaction parameter	β	plasticization factor
a	activity	c	concentration (g/ml)
M	molecular weight ($g\ mol^{-1}$)	A	virial coefficient ($cm^3\ mol\ g^{-2}$)
ΔC_P	Incremental change in heat capacity at T_g ($J\ mol^{-1}\ K^{-1}$)	m	mass (g)
w	weight fraction	t_D	drying time (s)
t_B	buckling time (s)	r	evaporation rate
D	mutual diffusion coefficient of solvent	$\alpha_0, \beta_0, \gamma_0$	Temperature dependent constants of Koningsveld and Kleintjens equation
Index			
1	nonsolvent	M	mixture
2	solvent	f	fiber
3	polymer	p	paraffin

1. Introduction

Electrospinning is a well-known and versatile technique to produce micro- and nanofibers. In this process very fine and continuous fibers are formed from an electrically charged jet of polymer solutions or melts when the electrostatic forces overcome the surface tension of the polymeric fluid [1, 2, 3, 4].

Electrospinning has been able to attract great attention because of a broad range of applications of electrospun fibers in drug delivery and tissue engineering [4-6], nanocomposite [4, 7], filtration [4, 8, 9], cosmetics [7], protective clothing [4, 10], developing super-hydrophobic surfaces [11, 12, 13, 14] and most recently oil absorption to cleanup the oil contaminations [15, 16].

Proof has shown that morphology of electrospun fibers plays an important role on their final application. Different processing parameters have been considered to influence the morphology of fibers during the process of electrospinning. These parameters can be categorized in three different groups:

- Electrospinning parameters including spinning voltage, working distance and feed rate [17, 18].
- Solution properties including solvent characteristics [14, 15, 19, 20], fluid elasticity [21], polymer concentration [15, 17, 18], polymer molecular weight [15, 18, 22], chain entanglement [23], surface tension of solution [18] and conductivity [18]
- Environmental conditions, i.e., temperature (T) as well as relative humidity (RH) [17, 22, 24-25, 26-27, 28], vapor concentration of solvent in electrospinning environment [28].

Porosity within electrospun fibers which makes them appropriate and promising candidates for elaborating super-hydrophobic surfaces [13, 14] as well as applications requiring high surface area such as filtration [8], catalytic systems [29] and membranes in sensing materials [30], can be considered as the prominent morphology of continuing and commercial interest which has been the main subject of recent scientific research [14-16,17, 22, 24, 26-27, 29-47].Therefore, numerous attempts have been made to extend electrospinning to introduce porous morphology in the structure of fibers. Articles reviewed revealed that porosity in electrospun fibers could be created by two dominant methods: indirect and direct methods.

Indirect methods require post-electrospinning treatments to form porosity such as selective dissolution of one component [33] and deposition of fibers in a cryogenic bath which is followed by drying in vacuo [34]. Gupta et al. [35] suggested a two-step approach to produce porous Nylon-6 fibers based on electrospinning Lewis acid-based complex solution of nylon-6 and $GaCl_3$ in nitromethane, which is implemented by removal of the $GaCl_3$ salt through soaking in water. Specifically, the advantage of this process is to produce highly

porous fibers and is balanced out by the need to post treatment as well as additional materials and facilities.

The direct methods, by which porous electrospun fibers are produced in a single step, are of great importance from practical point of view; moreover, the greater part of research has concentrated on this method. Upon examination of the various articles, the varieties of direct approaches that have been employed to reach porous structures within electrospun fibers can be classified as follow:

- Electrospinning at different levels of relative humidity [17, 22, 24, 26-27, 28, 44, 47]
- Using volatile solvents [12, 13, 17, 22, 31, 32, 40, 42, 47]
- Applying a mixture of two solvents (volatile/nonvolatile solvents [12, 14, 15, 16,17, 40, 47] or volatile/volatile solvents [42])
- Electrospinning a ternary system composed of nonsolvent/solvent/polymer (NS-S-P)with a certain ratio [39, 45]
- Changing concentration of polymer solution [15, 17, 40]
- Altering the relative rates of solvent evaporation to phase separation in a partially miscible solvent-polymer system [36-38]
- Immersing collector in a bath filled with a nonsolvent [43, 46]

Under humid conditions solvent volatility plays the pivotal role to induce the pores on the surface of electrospun fibers. For the case of solutions prepared from volatile solvents, solvent evaporation cools the jet surface on which water vapor is condensed and water droplets are formed at the interface of air and polymer solution phases. However, there is a practical limitation for solvent volatility. Using solvents with very high vapor pressure makes it very difficult to electrospin fibers because of the immediate formation of a skin on the surface of droplet on the needle [17]. A few studies have also looked at the pore formation on the surface of fibers produced from solutions of non-volatile solvents like polystyrene/dimethylforamide (PS/DMF) under humid condition. Demir [41] reported formation of surface pores of nanoscale diameter for fibers electrospun from PS/DMF solution under 35% relative humidity and room temperature. Recently, Nayani et al. [43] have been able to create nanoscale grooves on the surface of PS fibers along the fiber axis by collecting the electrospun fibers from PS/DMF in addition to PMMA/DMF solutions in a water bath.

Megelski et al. [17] discovered effect of electrospinning parameters such as spinning voltage, flow rate, working distance (distance between needle tip and grounded collector) on porous morphology. They observed an increase in the mean pore size with increasing flow rate and showed the pore size and pore formation are not influenced by changing working distance as well as spinning voltage.

Dayal and co-workers [36-38] investigated theoretically as well as experimentally the spatiotemporal evolution of fiber morphology during electrospinning process in the framework of the Cahn-Hilliard equation. They demonstrated it was possible to achieve porosity within the fibers by altering the relative rates of solvent evaporation to phase separation.

Exposing the polymer solution to the nonsolvent vapor atmosphere during the process of electrospinning may lead to diffusion-induced phase inversion by which the thermodynamic instability of polymer solution occurs. The thermodynamic instability is resolved by the separation into two phases: polymer-rich phase and polymer-lean phase. Polymer-rich phase forms a solid fiber matrix and polymer lean-phase leaves pores by leaching solvent and nonsolvent out of the system. Porous interior structure in electrospun fibers was recently observed by Pai et al. [24], who produced electrospun fibers from PS/DMF solution under relative humidity ranging from 11% to 43%. Increasing the relative humidity, in which phase separation is more probable, causes solidification to happen before buckling instability raised from compressive radial stresses, resulting fibers with smooth surfaces, as they established. Mass transfer paths superposed onto the ternary phase diagram of the system, predicting the occurrence of phase separation within the fibers, determine the mechanism of phase demixing as well as the evolution of structure. Using the mixture of nonvolatile/volatile solvent by some researchers [47] for electrospinning was a way to obtain different interior morphologies through different mass transfer paths.

However, the effective attempts on surface and interior morphologies of electrospun fiber, exhibiting co-continues pore morphology and structure transition of fiber surface, by superimposing the temperature and relative humidity of electrospinning atmosphere has not been reported. The main objective of our study is designed to present a comprehensive study on the formation of various surface and interior morphologies by systematic change of

both temperature and relative humidity of the electrospinning environment. Furthermore, impressibility of polymer solutions from ambient conditions during electrospinning process is disclosed in the framework of NS-S-P phase diagram at different temperatures. For this purpose, solvent volatility and phase behavior of solvent/polymer system in the presence of water vapor with different concentrations were investigated as dominant parameters dictating the contribution of environmental parameters to morphology evolution in electrospun fibers. Polystyrene was considered as a model polymer to be electrospun. Two solvents with low (dimethylforamide) and high (tetrahydrofuran) vapor pressure as well as their mixtures with different ratios, are employed to prepare electrospun fibers at various ambient conditions.

2. Experimental

2.1. Materials

Polystyrene (PS) ($M_W = 280000\ g/mole$, *Tg*=100 ℃), dimethylformamide (DMF), tetrahydrofuran (THF) and dichloromethane (DCM) of analytical grade used in this study were purchased from Sigma Aldrich, Inc. Deionized water was used as nonsolvent. Colorless Liquid Paraffin (C_nH_{2n+2} n=16~24) from BDH was used to measure the mass density of electrospun fibers. All materials were used as received without further purification.

2.2. Electrospinning setup

All electrospinning experiments were carried out in a chamber with controlled temperature (T) and relative humidity (RH) in high accuracy. A schematic representation of chamber has been illustrated in Fig. 1.

Insert Figure 1

The electrospinning chamber includes two boxes, inner box and outer box; the air between two enclosures creates an isolation gap which reduces the possibility of heat transfer, achieving a stable temperature and humidity in the inner box. The apparatus has been equipped with a conditioning box to provide air with desired temperature and humidity according to psychrometric charts. A cooling coil and heater control the temperature in the conditioning box. An

ultrasonic humidifier has been embedded in the chamber to increase the humidity level. To reduce the humidity levels, a condenser in conditioning box condenses the water vapors. An electrical fan was attached to circulate the air in the enclosures.

The special shape of the spinning chamber has been designed as such that the traveling path of jet of charged polymer solution to the collector is not disturbed by airflow. Arrows in Fig. 1 depict the path of air flow in the chamber. The temperature and RH of the chamber can be controlled between about 10 ℃ and 70 ℃ ($\pm 0.1^{\circ}C$) and from about 2% to 100% RH ($\pm 1\%$). Q-Series Duct Relative Humidity sensor (SIEMENS QFM2160) and the temperature sensor (Jumo from Germany, Push-In RTD Temperature Probe with Connecting Cable (902150)) were installed inside the chamber by which the relative humidity and temperature of the inner box are monitored and controlled. The electrospinning setup contains other components; a high voltage power supply (Gamma High Voltage ES 50P-10W) and a syringe pump (JZB 1800D Double Channel Syringe pump from China).

2.3. Preparation of electrospun fibers

Polystyrene solutions of concentration 20 wt.% were prepared by dissolving PS in DMF as well as THF and mixtures of THF/DMF with different volume ratios (50/50, 60/40 and 70/30) under gentle stirring at room temperature for at least 24 h. The prepared solution was loaded in a 10 ml glass syringe with metal needle.

For electrospinning of PS/DMF solutions, flow rate, working distance (nuzzle-to-collector distance) and voltage were 1 ml/h, 35 cm and 15 kV, respectively. While in the case of PS/THF and PS/(THF:DMF) solutions the above-mentioned electrospinning parameters were adjusted to be 1 ml/h, 20 cm and 30 kV.

Environmental conditions under which electrospinning was carried out contain three different temperatures (20 ℃, 40 ℃ and 60 ℃) and various levels of relative humidity (5, 10, 20, 30, 40, 50 and 60%) for each temperature. These conditions have been pointed in psychrometric chart (Fig. 2) where absolute humidity (ω) versus temperature for different levels of relative humidity (RH) are related according to Eq. 1 [48].

$$RH = \frac{\omega P_a}{0.622 P_g} \quad (1)$$

where P_g and P_a are saturation pressure of vapor in a given temperature and partial pressure of air, respectively.

Insert Figure 2

2.4. Ternary phase diagram

Ternary phase diagram of H_2O/DMF/PS and H_2O/THF/PS systems at different temperatures (20, 40 and 60 ℃) was determined by measuring the cloud points as well as calculating the free energy of the system.

2.4.1. Cloud point measurement

The cloud points of H_2O/DMF/PS and H_2O/THF/PS systems were measured at three different temperatures, i.e., 20 ℃, 40 ℃ and 60 ℃. For this purpose various concentrations of polymer solutions (2.5, 5, 7.5, 10, 12.5, 15 and 20 wt%) were titrated by water as nonsolvent to determine cloud points of solutions and during the titration process the temperature was kept constant. Titration was begun by introducing one droplet of titrant to polymer solution under stirring and continued by more droplets of titrant after the clear solution was observed for each added droplet. Otherwise, the occurrence of turbid point was regarded as the onset of cloud point and its composition was determined by calculating the partial amount of polymer (PS), solvent (DMF or THF) and nonsolvent (water) in the turbid mixture.

2.4.2. Theory

For thermodynamic description of the phase behavior in a ternary nonsolvent (1), solvent (2) and polymer (3) system, often Tompa extension [49] of the classical Flory-Huggins (FH) model is used. The Gibbs free energy of mixing, ΔG_m, in a ternary system can be formulated as Eq. 2.

$$\frac{\Delta G_M}{RT} = n_1 \ln \varphi_1 + n_2 \ln \varphi_2 + n_3 \ln \varphi_3 + n_1 \varphi_2 \chi_{12}(u_2) + n_2 \varphi_3 \chi_{23}(\varphi_3) + n_1 \varphi_3 \chi_{13} \qquad (2)$$

where R is the gas constant; T, the absolute temperature, respectively, n_i and φ_i are the number of moles, the volume fraction of component i, respectively. $\chi_{12}(u_2)$ is a generalized nonsolvent(1)/solvent(2) interaction function depending on the volume fraction $u_2 = \varphi_2/(\varphi_1 + \varphi_2)$ of a pseudo binary mixture [50, 51],

$\chi_{23}(\varphi_3)$ is also assumed as a concentration dependent interaction function of a binary solvent(2)/polymer(3) mixture, and χ_{13} is the nonsolvent(1)/polymer(3) interaction parameter, often assumed as a constant. The application of Eq. 2 requires three precisely and independently determined (binary) interaction parameters or interaction parameter functions. Knowing the interaction parameters between the three components, it is possible to calculate binodal, spinodal, tie lines, and critical points for the ternary system. More information about the mathematical/numerical treatment may be found, e.g. in Ref. [52].

2.4.2.1. DMF/PS and THF/PS interaction parameter

Vapor pressure osmometer (VPO) was used to determine the DMF/PS and THF/PS interaction parameters (χ_{23}). This technique works based on vapor pressure of solvent. Such that the equilibrium vapor pressure of solvent in the polymer solution is smaller than that of pure solvent at the same conditions. This difference is a function of mole fraction of polymer and can be calculated by VPO. A VPO device contains two thermistors, which have been placed in the measuring chamber saturated with solvent vapor. A drop of polymer solution is placed on the surface of one of thermistors and a drop of solvent is placed on the surface of another thermistor. The condensation from the saturated atmosphere warms the thermistor containing polymer solution drop. This attained temperature difference between two thermistors is transferred into a voltage difference ($\Delta\Phi_{el}$) which is directly related to the osmotic pressure π, as given by Eq. 3 [53].

$$\frac{\pi}{RT} = \frac{\Delta\Phi_{el}\rho_2}{1000K} \tag{3}$$

where *K* and ρ_2 are calibration constant and solvent density, respectively. In the present work a vapor pressure osmometer (Knauer K-7000, Germanny) was calibrated by solutions of benzil in DMF and THF of various concentrations (0.21-0.84 wt.%) and then loaded by each pure solvents for measuring the voltage difference ($\Delta\Phi_{el}$) between pure solvent and polymer solutions of different concentrations ranging between 3 to 20 wt.%. The averaged values of 5 times reading for $\Delta\Phi_{el}$ were reported as input of Eq. 3. The osmotic pressure of polymer solutions can be described by virial expansion as Eq. 4.

$$\frac{\pi}{RT} = \frac{1}{M_3} c_3 + A_2 c_3^2 + A_3 c_3^3 + ... \quad (4)$$

where c_3 is the concentration of the polymer (expressed in g/ml), M_3 is the molecular mass of the polymer, and A_2 and A_3 are the second and the third osmotic virial coefficients of the polymer in the solvent, respectively. The concentration dependency of the interaction parameter is expressed by Eq. 5.

$$\chi_{23}(\varphi_3) = a_0 + b_0 \varphi_3 \quad (5)$$

where $a_0 \equiv (1/2) + b_0 - \rho_3^2 v_2 A_2$ and $b_0 \equiv -(1/2)\rho_3^3 v_2 A_3$. ρ_3 and v_2 denote to polymer density and solvent molar volume, respectively.

2.4.2.2. Water/PS interaction parameter

Water uptake measurement at three different temperatures (20 ℃, 40 ℃ and 60 ℃) was used as a simple and well-known method to evaluate the water/PS interaction parameter (χ_{13}) based on GRP model suggested by Karimi et al. [54]. According to this model χ_{13} can be evaluated using Eq. 6.

$$\frac{\Delta\mu}{RT} = \ln a_1 = \beta[\ln(\varphi_1) + (1-\varphi_1)] + (1-\beta) \times \left[\ln\left(\frac{\varphi_1}{\varphi_0}\right) \right] + (1-\varphi_1)^2 \chi_{13} \quad (6)$$

where a_1, β and φ_1 are the water activity, plasticization factor and volume fraction of absorbed water, respectively. φ_0 ($\varphi_0 = \varphi_{FV} - \varphi_1$) represents the volume fraction of unoccupied spaces into the polymer and φ_{FV} is the fractional free volume of the polymer. Details of the calculation are presented in the Appendix.

Water uptake was evaluated for PS films. For this purpose, PS films were cast from PS/DCM solutions by dissolving a given amount of PS granule in DCM under gentle stirring at room temperature for about 24 h until a clear solution with a polymer concentration of 20 wt.% was obtained. The solution was then kept at room temperature for 24 h to be degassed. The degassed solution was cast using a knife with a slit of thickness of 200 μm and then placed into the atmospheric condition for evaporating the solvent. To remove the residual solvent the cast films were dried for 48 hours under vacuum at 90℃. The final thickness of prepared films was measured to be 40 μm.

To measure water/PS interaction parameter at temperatures of interest, prepared PS films of given weight were immersed in water bath with controlled temperature (±0.5 ℃). Soaking in desired times, films were pulled out from water and weighed after shortly contacted with tissue to dry surface adhered water. This process was repeated until a constant wetted weight was achieved (about 3-4 days). Knowing the dried weight of polymer film makes it possible to calculate the volume fraction of absorbed water that is required to calculate the water/PS interaction parameter.

2.4.2.3. H_2O/DMF and H_2O/THF interaction parameter

The data set of binary interaction parameter of H_2O/DMF system was collected from literatures [55, 56] and presented based on Koningsveld and Kleintjens model (Eq. 7). It was assumed these data were correct. In the case of H_2O/THF system, parameters required for evaluating Eq. 7 were calculated based on UNIFAC method at temperatures of interest. The values obtained for $\chi_{water/THF}$ at 20 ºC according to UNIFAC approach, compares favorably with literature [57].

$$\chi_{12}(u_2) = \alpha_0 + \frac{\beta_0}{1-\gamma_0 u_2} \tag{7}$$

where α_0, β_0 and γ_0 are temperature-dependent constants .

2.5. SEM analysis

Scanning Electron Microscope (SEM) (TESCAN series VEGA 2007 from Czech) evaluated surface morphology along with cross-section of electrospun fibers as well as their diameter distribution from captured images at 30 kV acceleration voltage(s). Before SEM analysis samples were coated with a 30 nm layer of gold.

2.6. Measurement of fractional pore volume of electrospun fibers

Density of electrospun fibers was considered as an accurate and versatile criterion to examine and determine the interior porosity of produced fibers. For this purpose fibers were mixed with liquid paraffin in a glassy vessel with calibrated volume of 1.8821 cm^3 to form an integrated composite. Liquid paraffin was chosen as matrix due to its non polar and hydrophobic nature, two essential factors for complete wetting of polystyrene fibers. In addition, large paraffin molecules are not susceptible to diffuse in the interior porous structure

of fibers. Knowing the total volume of composite (V_C) corresponding to the volume of vessel and mass of electrospun fibers (m_f) and then measuring the mass of matrix, i.e., fiber/paraffin mixture (m_M), allows one to calculate the density of produced fibers as given by Eq. 8.

$$\frac{1}{\rho_M} = \frac{w_f}{\rho_f} + \frac{w_p}{\rho_p} \tag{8}$$

where w_i and ρ_i ($i = f$:fiber and p :paraffin) are weight fraction and density of component *i*, respectively. Eq. 9 was applied to compute the fractional interior pore volume (FPV) using specific volume data ($\upsilon = 1/\rho$).

$$FPV = \frac{\upsilon_f - \upsilon_{ref}}{\upsilon_f} \tag{9}$$

In Eq. 8, υ_{ref} denotes to specific volume of granule with no interior porosity. υ_{ref} was measured to be 0.95 cm^3/g which is in good agreement with that provided by manufacturer.

3. Results and discussion

3.1. Ternary phase diagrams

As described by several authors [17, 22, 24, 40, 41, 47] vapor-induced phase separation (VIPS) is the dominant mechanism controlling morphology of fibers electrospun at humid environment. Water is a nonsolvent for PS, hence, solutions of PS may thermodynamically become unstable and then undergo phase separation when it is exposed to water vapor. Thereby, phase diagram of nonsolvent/solvent/polymer system is an effective tool to explain morphology of produced fibers. In this work, ternary phase diagrams of H_2O/DMF/PS and H_2O/THF/PS for three different temperatures, i.e., 20, 40 and 60 ℃, were constructed by means of Flory-Huggins theory and its superposition onto experimentally measured cloud points, as shown in Fig. 3. All parameters required for calculation are listed in Table 1.

Insert Table 1

The values of 0.499 and 0.470 obtained for $\chi_{DMF/PS}$ and $\chi_{THF/PS}$, respectively, which is in good agreement with literature data [58, 59], were considered to be constant. Our calculations on VPO data show that three-body interaction is insignificant in both binary mixtures, presenting a concentration-independent interaction. Additionally, no significant temperature-dependency is considered for solvent/polymer interaction parameter as described by Karimi et al. [53].

Insert Figure 3

3.1.1. Effect of interaction parameters

The impact of all three essential interaction parameters required for predicting phase behavior of ternary system differs from each others. H_2O/PS is the common pseudo-binary mixture of both H_2O/DMF/PS and H_2O/THF/PS systems and a same value of χ_{13} are used for calculation. In addition, no significant difference was observed for interaction parameters of DMF/PS and THF/PS binary systems. It is obvious that such small difference in solvent/PS interaction parameters cannot contribute to change remarkably the location of the miscibility gap; our claim was tested by changing the solvent/PS interaction parameter while other interaction parameters were kept unchanged. Consequently, the difference in phase behavior of H_2O/DMF/PS and H_2O/THF/PS can be attributed to χ_{12} interaction parameters. Since it has been seen [56] in the analysis of vapor-liquid-equilibrium data with the models of Gibbs free energy mixing the χ_{12}-value changes with the volume fraction of components, this parameter is considered concentration dependent. Fig 4 shows the value of χ_{12} for the whole range of concentration, presenting remarkably higher values for THF rather than DMF at all composition range, which denotes in comparison with DMF, THF has relatively low tendency to mix with water. Therefore, more nonsolvent is needed for liquid-liquid demixing corresponding to small miscibility gap for H_2O/THF/PS. Altena and Smolders [51] also reported this finding. In consequence of aforementioned points, a larger miscibility area for H_2O/THF/PS in comparison with H_2O/DMF/PS system is observed, as seen in Fig. 3.

Insert Figure 4

3.1.2. Effect of temperature

At a first glance it shows that the binodal curves as well as cloud points are severely affected by temperature of polymer solution. Higher temperature shifts the binodal curve toward nonsolvent-polymer axis corresponding to larger miscibility area. Commonly, the amount of shift depends on binary interaction parameters of the mixture. χ_{23} exhibits poor dependency to temperature and therefore, the solvent/polymer interaction parameter can not greatly contribute to change the binodal position with temperature. Same argument exits for χ_{12}. In contrast to χ_{23} and χ_{12}, the most probable interaction parameter affecting phase behavior of the ternary system under temperature variation is χ_{13} which should be determined using GRP model developed by Karimi et al. [54]. Altena and Smolders [51] also showed that miscibility gap is strongly affected by nonsolvent/polymer interaction parameter (χ_{13}), showing a higher temperature-dependency than others.

3.1.3. Mass transfer path

Interplaying the mass transfer and VIPS process is an essential aspect of phase behavior of the mixtures, describing the morphology change in fibers electrospun at humid conditions. In a ternary phase diagram as depicted in Fig. 5, three regions including homogeneous, meta-stable and unstable region exist which are divided by the binodal and spinodal curves. Composition at the metastable region goes to separate via nucleation-and-growth (NG) mechanism, resulting in isolated cellular pores embedded in polymer matrix if the polymer-lean phase is nuclei. While at the unstable region it separates via spinodal decomposition (SD) mechanism, resulting in co-continuous interconnected networks of pores [60]. No phase separation is taken for solution under mass transfer if its composition is changing in homogeneous region. With this in mind, the mechanism through which morphology evolution is precedes depends on the path that the composition of polymer solution changes in homogeneous region. Three possible paths have been typically drawn in this area (Fig. 5). The mixture through the path I is going to solidify compactly while the two other paths (II and III) enter into metastable or unstable regions in which a porous morphology has been finally obtained.

Insert Figure 5

In the case of forming an electrospun fiber under humid conditions in which a phase separation may take place, considering mass transfer path is fitting our discussion on morphology evolution. Choosing DMF and THF as nonvolatile and volatile solvents, respectively, provided two different rates of evaporation in H_2O/DMF/PS and H_2O/THF/PS systems. At constant rate of water penetration, the former system tends to find a path like type III, while the latter system would act as the path type I. Varying the level of relative humidity, absolutely, changes directly the activity of water at gaseous phase influencing on rate of water penetration and also the compositional path.

3.2. Interior structure of electrospun fibers

3.2.1. PS/DMF solution

Fig. 6 represents microphotographs of fractured cross-section of PS fibers electrospun from 20 wt.% PS/DMF solutions at different levels of relative humidity (RH) ranging from 20% to 60% and temperature of 20 ^{o}C. Two types of interior morphology, non-porous (Fig. 6a) and porous (Figs. 6b-e), could be discerned for these fibers. Fig. 6e shows the cross-section of fiber produced at RH equal to 60% (the highest value of RH at this study), a porous structure with pore-connectivity is observed. The interior porosities of fibers reduce by decreasing the RH. Besides, a coarse polymer phase is cleared gradually from higher to lower RH; finally, a dense cross-section for fiber is developed at RH of 20% (Fig. 6a).

Insert Figure 6

Exchanging solvent and nonsolvent through the interface between polymer solution and humid air is beginning after the solution jet enters into the electrospinning box. Depending on the nonsolvent concentration jetted solution may experience phase separation or not. Phase separation process could accounts for porous morphology formation while dense cross-section gives evidence confirming no phase demixing in the skeleton of fibers. Through the path crossed the binodal curve, polymer solution becomes thermodynamically unstable, bringing the composition of the electrospinning jet into the phase demixing region where polymer-rich and polymer-lean domains can be

emerged. The former makes the polymer matrix while the latter develops eventually into pores. As evident from Fig. 6 depending on the level of RH, electrospinning under humid atmosphere permits fibers to create porosity in their structure by means of SD mechanism, or to solidify without porosity by passing through the miscibility region of three-angle phase diagram.

Temperature is believed to influence the morphology of electrospun fibers by affecting electrospinning atmosphere (according to psychrometric chart represented in Fig. 2), expansion of miscibility area (Fig. 3) and rate of mass transfer across the interface between solution jet and gaseous phase. Figs 7 and 8 show the SEM images for fractured cross-section of fibers electrospun at temperatures of 40 ^{o}C and 60 ^{o}C and different RH as chosen for temperature of 20 ^{o}C. Increasing RH, morphology transition from non-porous to porous structure in fibers did occur at certain RH, depending on operating temperature. As cleared in microphotographs, certain RH for morphology transition shifts to higher value if the temperature of process goes up.

Insert Figure 7

Insert Figure 8

Increasing the temperature of electrospinning process increases the value of water dissolved into the polymer solution jet meaning the expanse of miscibility area in phase diagram. Thus, a delayed phase inversion can be adopted for the solution electrospinning at higher temperature, resulting a grown polymer-rich phase and lower value for interior porosity. On the other hand, keeping RH constant the solvent outflow at higher temperatures becomes faster while nonsolvent inflow rate remains constant, moving the mass transfer path away the binodal curve and consequently reducing the probability of phase demixing. Further evidence may be supported by the solid cross-section of fibers produced at 60 ℃-30% RH (Fig. 8c). At this conditi on water absorbed by the jet is not high enough to induce phase separation, while at 20 ℃ and 40 ℃, such level of RH (30%) can bring about porous interior morphology (Figs. 6b and 7b). Comparing the SEM image of three samples, produced at the same absolute humidity (concentration of water in electrospinning atmosphere), i.e., 20 ℃-60%RH, 40 ℃-20%RH and 60 ℃-10%RH as evident from Fig.2, reveals that

there exists a tremendous differences in their interior morphology (Figs. 6e, 7a and 8a). Similar behavior can be recognized for fibers electrospun at conditions of 40 ℃-50%RH (Fig. 7d) and 60 ℃-20%RH (Fig. 8b). These observations clarify that the value of water cannot be an accurate factor describing the morphology evolution of fiber; therefore, the relative humidity should be considered as chemical potential of water instead of absolute humidity to rationalize morphology of obtained fibers.

Probing the interior morphology of fibers gives clear indication of the existence of interconnected networks of pores forming the interior structure of porous fibers. Hence, developing of interior porosity in PS/DMF electrospun fibers can be best described by spinodal decomposition as a consequence of water intake from vapor phase known as vapor-induced phase separation (VIPS). It is a reasonable conjecture that environmental parameters affect fiber interior morphology by influencing VIPS mechanism.

In the case of fibers with porous interior morphology, it appears that their interior porosities vary by environmental conditions. Fractional interior pore volume (*FPV*) (Fig. 9) evaluated at different ambient conditions, gives the reader general idea of the interior porosity of porous fibers. According to Fig. 9, as expected, fibers with dense cross-section (Fig. 6a, Fig. 7a, Figs. 8b, c) have *FPV* comparable to PS granule verifying no phase separation has been occurred within these fibers. Additionally, *FPV* of produced fibers is affected by both temperature and relative humidity.

Insert Figure 9

At constant temperature, *FPV* of produced fibers shows an ascending order with the relative humidity of electrospinning chamber (Fig. 9). Although some inconsistencies are observed particularly at RHs of 50% and 60%, but such ascending trend is verified for all working temperatures.

3.2.2. PS/THF and PS/THF:DMF solutions

Interior morphology of fibers electrospun from 20 wt.% solutions of PS/THF at different ambient conditions has been explored by SEM images and presented in Fig. 10. Microphotographs in this figure show that all fibers electrospun from PS/THF solutions have dense cross-section regardless of operating conditions,

verified by density measurement; fractional interior porosity of fibers was measured in the range of 0.04 to 0.08 which confirms dense morphology for cross-section of these fibers. Therefore, it is reasonable to postulate that phase separation has no contribution on the evolution of interior morphology of fibers electrospun from PS/THF solutions. As previously shown in Fig. 3, the miscibility area of H_2O/THF/PS system is larger than H_2O/DMF/PS system, meaning that higher value of water needs to diffuse into the solution jet for crossing the binodal curve. Besides, higher vapor pressure of THF than which of DMF, involving in solvent evaporating rate during the electrospinning process is the other important factor that should be considered. As a result, these two factors control the mass transfer path to pass through the miscibility area without crossing the binodal curve and then the solution jet solidifies with a dense morphology.

Insert Figure 10

Non-circular cross-section as observed in Fig. 10 is another feature of PS fiber electrospun from solution of THF. This is claimed that the reason is due to buckling instability that occurs during the solvent evaporation. Under high compressive stresses, where the actual compressive stress at the point of failure is less than the ultimate compressive stresses, the skin may experience lateral deformation due to elastic instability. In order to describe the buckling instability, two characteristic times, i.e., drying time (t_D) and buckling time (t_B) were proposed by Pauchard et al. [61, 62] and applied by Pai et al. [24] to explore this phenomenon in polymer solution jet. Both of these times are inversely proportional to evaporation rate (r), while the t_B is directly related to mutual diffusion coefficient (D) of solvent. Both solvent evaporation rate and mutual diffusion coefficients [63] are direct functions of temperature. Regarding SEM images of Fig. 10, it can be easily seen that at low temperatures such as 20 ℃ where both r and D descend, ribbon-like morphology is dominant regardless of operating RH (Fig. 10a,b). It is believed to be owing to reduced r and D, which makes t_B shorter than t_D. By increasing temperature to 40 ℃ which is close to the boiling point of THF (~66 ℃) , both r and D rise. In the case of t_B it seems the effect of increased D on t_B is more pronounced than increased r, making t_B comparable to t_D. Therefore, As shown in Figs. 10c,d approximately

circular cross-sections can be observed for fibers electrospun from PS/THF solution at 40 ℃. These results compare favorably with model suggested by Pai et al. [24] who proved that cross-section of fibers could adopt different shapes to account for the influences of both drying and buckling events.

As stated earlier, the rate of phase separation taken place in polymer solution jet undergoing solvent and nonsolvent exchange through the solution/vapor interface, goes faster to solidify the jet. The time taken to account for evolving the phase separated morphology is considered as third characteristic time for balancing the compressive stresses involved in skin formation. This is developed by Pai et al. [24] and used to describe the morphology of electrospun fibers. We added DMF as nonvolatile solvent to PS/THF mixture to increase the buckling time during the electrospinning process and decrease the time for phase separation. Fig 11 represents SEM images of fractured cross-section for PS electrospun from solution of THF:DMF with ratio of 100:0, 70:30, 60:40, 50:50, and 0:100 at conditions of 40 ºC-60% RH.

Insert Figure 11

Using a mixed THF:DMF of 70:30 as solvent for electrospinning causes an increase for buckling time and a decrease for solidification time. At presence of DMF as nonvolatile solvent, depending on DMF content buckling time is increased as evidenced by formation of rigid skin under phase separation which has higher rate than when DMF is absent. Under this situation a porous interior structure is developed and a collapsed bean-shaped cross-section is appeared (Fig. 11b). Increasing the DMF content to 40%, this collapsed cross-section is replaced by rather circular one having irregularly jagged edges (Fig. 11c). By further increasing DMF content, the phase separation precedes both buckling and drying events and fibers with porous and complete circular cross-sections are expected (Fig. 11d, e). The measured values for interior porosity confirm the explanations in which *FPV* can be tailored by DMF content (Fig. 12). On the other hand, as high as DMF content, as high as *FPV*.

Insert Figure 12

3.3. Surface morphology of electrospun fibers

3.3.1. PS/DMF solution

SEM images captured from surface of fibers electrospun from PS/DMF solutions (20 wt.%) at different environmental conditions have been shown in Fig. 13.

Insert Figure 13

Focusing on Fig. 13 reveals three different surface morphologies, wrinkled, non-porous and porous, could be discerned for fibers, tailored by tuning environmental parameters (temperature and RH), while other electrospinning parameters have been kept constant.

As will be discussed later, electrospinning at low-RH (5% and 10%) regardless of working temperature, leads to bead-on-string morphology with high bead density and very fine fibers having too slight roughness on their surfaces (Fig. 13a-f). These fibers are 200-500 nm in diameter. Increasing RH to values of 20% and more creates fibers which benefit from a variety of surface features.

At constant temperature, wrinkled surface becomes dominant morphology at a certain range of RH, depending on temperature. At temperature of 20 ^{o}C, for instance, the surface of fiber is wrinkled for RH of 10% and 20% (Figs. 13d, g), while this limits to RH of 20% at temperature of 40 ^{o}C (Fig. 13h) and to RH of 20% and 30% at temperature of 60 ^{o}C (Fig. 13i, l). In addition, at conditions of 60 ^{o}C 40%RH, some fibers with wrinkled surfaces can be found (not shown here) but the dominant morphology contains surface with no wrinkles on it. At all temperatures, the surface morphology changes from non-porous to wrinkled structure and then transfers from wrinkled to porous structure. Totally, this idea is coming to mind that two transitions take place in surface morphology of fibers if RH is varying; by increasing RH, morphology transition in surface of fiber can be sorted according to

non-porous → wrinkled → porous

A very important practical map of structural transitions in surface as well as interior morphologies of fibers electrospun under different levels of RH and temperatures has been systematically marked on temperature-relative humidity chart by exploring Figs 6, 7, 8 &13. This has been revealed in Fig 14. In this diagram, region 1 belongs to bead-on-string morphology with very fine fibers. Fibers located in this region benefit from non-porous structure in both surface

and cross-section. Region 2 is related to fibers with wrinkled surface and non-porous cross-section. Finally, region 3 is occupied by fibers with porous cross-section and either non-porous or porous surface depending on temperature and relative humidity.

Insert Figure 14

Analysis of SEM images for fiber surface, assigning as porous morphology, shows a regular change in pore size ranging from about 43 nm to 148 nm which are dependent on both RH and temperature of electrospinning atmosphere. The mean value of surface pore diameter of fibers electrospun under different environmental conditions has been listed in Table 2. At a constant temperature, density of surface pores diminishes if RH is increasing from 30% to 60%. Similar descending order for pore density is also observed when temperature rises from 20 ℃ to 60 ℃ at constant RH. Consideri ng SEM images (Fig. 13), it is obvious that surface pores with highest density belong to fibers produced at 20 ℃ and RH of 30% and 40% as well as those electr ospun at 40 ℃-60%. Other fibers especially those produced at 60 ℃ can be categorized as fibers with solid (pore-less) surface.

Insert Table 2

The cause of buckling phenomena develops from elastic instability at the layer undergoing vitrification and leads to form a wrinkled surface morphology in electrospun fiber at certain range of RH and temperature. The samples having wrinkled surface (Fig. 13d, g-i, l) exhibit nonporous cross-section (Figs. 6a, 7a, 8a-c), meaning no phase separation takes place during the process of electrospinning. Such observation was also reported by Pai et al. [24] who found electrospinning of 30 wt.% PS/DMF solution at relative humidity of 15% and 22% both at room temperature leads to wrinkled surface morphology.

In order to explain the factors involving in development of different types of surface morphology, three characteristics times, i.e., buckling time, drying time, and time for phase separation, as previously mentioned, should be taken into account. As solution jet entered into the electrospinning box, phase separation takes place if the solution becomes thermodynamically unstable. This

phenomenon known as VIPS occurs when an enough amount of water vapor diffuses into the solution until the composition path crosses binodal curve on phase diagram. At this condition, two phenomena compete against each other. These are liquid-liquid phase separation and interfacial tension in the solution-air interface. The former causes pore formation onto the surface while the latter tends to bring the polymer-rich phase in contact with air. On the other hand, solvent evaporation moves the composition path of solution jet surface toward a higher polymer concentration before crossing the binodal curve, bringing the solution composition probably into the meta-stable region. This is an argument for considering the probability of nucleation and growth mechanism for pore formation onto the fiber surface rather than spinodal decomposition mechanism which was the only acceptable process for pore evolution into the fiber. Additionally, it seems the packing density of surface pores is involved to the viscosity of polymer-rich phase, which is controlled by composition path settled on homogeneous region of phase diagram. At lower RH, the composition path is moved toward the higher polymer content for solution jet before crossing the binodal curve corresponding to higher viscosity for polymer solution. While at higher values of RH, an opposing result, i.e., a relatively low viscosity for polymer solution is expected. As a result, the polymer-rich phase generated at high RH exhibits small resistance against interfacial tension which is eventually followed by low surface porosity. A similar explanation could be proposed for reducing surface pores by increasing temperature in which polymer-rich phase is generated at higher polymer concentration. These claims conflict with SEM images obtained from surface of fibers produced at 40 ºC-60%RH (Fig. 13t). One might presume that RH of 60% is an optimum value to obtain surface porosity at 40 ºC. This requires further investigation. The influence of interfacial tension in the solution-air interface on the surface porosity of membranes prepared by VIPS process was also reported by Tsai et al. [64].

Finally, a critical diameter is essential for surface wrinkles to form and in the case of thin fibers, solvent drying precedes both phase separation and buckling processes and formation of wrinkled surface is precluded.

3.3.2. PS/THF and PS/(THF:DMF) solutions

PS was electrospun from a volatile solvent, i.e., THF at two different temperatures, 20 and 40 ℃ and relative humidity of 20% and 60%. SEM images of these fiber surfaces have been presented in Fig. 15.

Insert Figure 15

From microphotographs of Fig. 15, it becomes clear that different surface structures with various porosities can be observed for fibers electrospun from PS/THF solutions in contrast to fibers obtained from PS/DMF solutions. When chamber temperature is sufficiently low, e.g., 20 °C, ribbon-like morphology with different porosity is prevalent (Figs. 15a, b). Raising the temperature to 40 ℃, leads to formation of both ribbon-like surface (Fig. 15c) and microscale holes (Fig. 15d) on the surface of fiber depending on RH.

Size and shape of nanopores on the surface of PS fibers electrospun from THF solutions are another points which severely influenced by both temperature and humidity. Nanopores formed at 20 ℃-20% RH (Fig. 15 a) are relatively uniform in size with average diameter of 104 nm but those emerged at 20 ℃, 60% RH (Fig. 15b) transform to a variety of shapes such as tear-like and circles with different diameters. In this case, the value of 182 nm was measured as the mean diameter of surface pores. At 40 ℃-20% RH, ve ry small circular pores (67 nm in diameter) can be detected on the fiber surfaces (Fig. 15c). By more increasing the RH to value of 60%, large pores (256 nm in diameter) with incredibly ordered arrays are formed on the surface of fibers (Fig. 15d).

Formation of pores onto the surface of electrospun fiber under humid condition when a volatile solvent like THF is used, goes in different manner as discussed for nonvolatile solvent like DMF. Rapid evaporation of solvent from the surface of polymer solution jet makes it cold and susceptible for condensation of water vapor. Condensed water droplets act as hard spheres which after drying leave an imprint on the surface, calling breath figure patterns which are widely studied in various articles [65-69]. Our experiences on fibers electrospun from THF solutions showed that at constant temperature, the mean diameters of surface pores increase with RH (Fig. 15). In fact, increasing RH means higher amount of water vapor in the atmosphere and then more water droplets are prone to condense on the fiber surface under evaporative cooling. In addition, the probability of coalescence of droplets and forming larger pores rises. On the

other hand, coalescence of some water droplets is the main reason of a broad distribution of pore diameter at high RHs (Figs. 15b, d). This matches findings of Peng and coworkers [67] who used linear polystyrene without any polar end group to examine breath figure formation. But they were not able to obtain such highly ordered arrays of pores within films cast from linear polystyrene.

At 40 ℃ compared to 20 ℃, the amount of water vap or at corresponding RHs is higher (Fig. 2). However, at higher temperatures, the driving force of concentration reduces. It is why the pores evolved at 40 ℃-20% are significantly smaller compared to those formed at 20 ℃-20%. At condition of 40 ℃-60%, the absolute humidity is remarkably higher than condition of 20 ℃-60% (Fig. 2) which outmatches the reduced driving force of condensation. Additionally, higher evaporation rate of THF at 40 ℃ rather than 20 ℃, motivates further the evaporative cooling of fiber surface which is essential to breath figure formation. Therefore, a superficial layer of highly ordered array of pores is appeared on the surface of fibers electrospun from PS/THF solution (Fig. 15d). The developed pattern on the surface of electrospun fiber from linear PS/THF at 40 ℃-60% resembles film produced by Park et al. [65] from solution of monocarboxylated end-functional polystyrene (PS_mCOOH) in THF.

Applying the mixture of THF/DMF as volatile/nonvolatile solvents, results in fibers with rough and pore-less surfaces, as displayed in Fig. 16. In other words, addition of DMF has prevented the surface pores to form while such surface morphology is very common in fibers electrospun from pure THF (Fig. 16a). By diminishing THF content in the solvent mixture, surface morphology changed from porous collapsed ribbon-like structure to nonporous surface. Conclusively, it can be said that surface structure of fibers produced from PS/(THF:DMF) systems is determined by solvent composition.

Insert Figure 16

3.4. Formation of bead in process of electrospinning at different environmental conditions

Beads or bead-on-string morphologies are unfavorable when a stable process of electrospinning is aimed. However, it becomes important for specific applications such as making super hydrophobic surfaces [12]. Here, two factors, i.e., temperature and RH related to appearance/disappearance of beads are

discussed for PS/DMF system. These factors are highlighted rather than other factors that are argued strongly in various articles [70].

Microphotographs of PS mats electrospun from 20 wt.% PS/DMF solutions at different temperatures and RH have been sorted in Fig. 17. Fibers electrospun at RH of 5% as well as 10%, regardless of working temperature, exhibit bead-on-string morphology with high bead density while those produced at other environmental conditions show either beadless or strictly speaking low bead density appearance. The bead-suppression as observed by increasing the RH is also supported by increasing the temperature of electrospinning.

Insert Figure 17

During the process of electrospinning under humid condition, penetrating water into the polymer solution jet raises the thermodynamic instability and evaporating solvent from that increases the polymer concentration of jet. Both events lead to raised viscoelastic forces. As a result, the capillary instability which is responsible for bead formation [18] is prevented and hence bead formation is suppressed. In contrast, at low-humidity, small amount of water diffused into the solution jet causes a delayed solidification and consequently capillary instability overcomes viscoelastic stresses, resulting bead with high density to develop.

3.5. Diameter of fibers electrospun at different environmental conditions

From SEM images of produced webs, diameter of fibers electrospun from PS/DMF solution was determined. For this purpose, diameters of 50 randomly selected fibers were measured using an image analysis software and the mean value was chosen to present. Plotting the change of fiber diameter versus RH of electrospinning chamber for different temperatures has been illustrated in Fig. 18. Diameter of electrospun fibers is linearly increased if the value of RH increases. Temperature of electrospinning does not affect the diameter of fibers considerably; only a small change is observed at RH=60%.

Insert Figure 18

The polymer-rich phase formed after separating the solution into two phases under thermodynamic instability, is a concentrated solution which solidifies under mass transfer faster than when no phase demixing takes place. This is an essential event, starting at the surface of polymer solution and developing into the solution jet. Since electrospinning jet can no longer be elongated after solidification, when solidification is expedites as a result of high water vapor concentration at high values of RH, there is little time for jet to elongate due to Coulombic forces and whipping instability during traveling to collector. Hence, further thinning of jet is suppressed and fibers with large diameters are expected. The argument is verified by calculations of Pai et al. [24]. They predicted the mass transfer path for 30 wt.% PS/DMF solution during electrospinning and demonstrated that raising the relative humidity causes the mass transfer path to intercept the binodal curve in a shorter time, consequently, solidification becomes faster at higher RH. Increment of fiber diameter with RH can also be explained in the context of dielectric constant. As discussed by Luo et al. [71], dielectric constant is defined as the ability of a substance to store electrical charge. It seems reasonable to postulate that increased RH corresponds to reduced dielectric constant of electrospinning jet. Because as argued by Kim et al. [26] increased RH makes the charged jet more prone to discharging as a direct consequence of higher conductivity of water vapor in comparison with air. Hence, it is expected to observe an ascending order for fiber diameter as RH rises due to decreased repulsive Coulombic forces. Similar behavior was recently reported by Luo et al. [71] who examined how diameter of electrospun polycaprolactone fiber is affected by dielectric constant of solvent.

4. Conclusion

Porous fibers were produced in electrospinning process under controlled humid condition (5, 10, 20, 30, 40, 50, and 60%) and temperatures of 20, 40, 60 ^{o}C for PS/DMF, PS/THF, and PS/THF:DMF systems. Phase behavior of H_2O/DMF/PS and H_2O/THF/PS systems at working temperatures was determined as an effective tool to explore the morphology evolution within the electrospun fibers. DMF as non-volatile solvent was capable to build up the porosity into the fiber while THF as volatile solvent was responsible for developing porosity onto the fiber surface. Pore formation concerning to former case is arisen from the

thermodynamic instability of polymer solution undergoing penetration of water from gaseous phase, so-called vapor-induced phase separation (VIPS), while the latter case is described by breath-figure formation, as a result of water condensation from gaseous phase because of evaporative cooling of the jet surface. Wrinkled surface morphology, another feature of fibers, was obtained from PS/DMF solutions which developed at certain levels of relative humidity and temperature. Increasing the relative humidity and temperature of electrospinning conditions leads to bead suppression which can be described by rheological property of polymer solution undergoing solvent evaporation and water penetration. Diameter of electrospun fibers were increased if the relative humidity and temperature were increased. Gelation and then solidification, the last sequences of forming structure, were the reason to prevent the elongation of jet in the process. Therefore, overcoming the viscoelastic stresses to capillary instability causes not only resulting bead-free web, but also increasing the diameter of fibers.

Appendix: Calculation of water/PS interaction parameter based on GRP model

In GRP model φ_{FV} can be estimated by Eq. A.1.

$$\varphi_{FV} = \frac{V_{FV}}{V_{total\_PS}} = \frac{1/\rho_{PS} - 1/\rho_{PS}^{*}}{1/\rho_{PS}} \quad (A.1)$$

where *V* denotes to volume (cm^3). ρ_{PS} and ρ_{PS}^{*} are PS density at temperature *T* and hard-core density of PS (expressed in Table A.1), respectively. ρ_{PS} can be computed by Eq. A.2 [65].

$$\rho_{Ps}(T) = \rho_{PS}^{*} \exp(-\alpha_{PS} T) \quad (A.2)$$

In Eq. A.2 α_{PS} stands for the thermal expansion coefficient of PS (reported in Table A.1). In GRP model, β, plasticization factor, is a function of temperature defined as Eq. A.3.

$$\beta = \frac{T_{gM} - T_{g3}}{T - T_{g3}} \quad (A.3)$$

where T_{gM} and T_{g3} are glass transition temperatures of mixture and polymer. *T* is the operation temperature. The Eq. A.3 is only valid for $T_{gM} > T$. For $T_{gM} \le T$, $\beta = 1$. On the other hand β ranges between 0 (for a completely glassy like state) and 1 (for a completely rubber like state). T_{gM} can be calculated according to Eq. A.4.

$$T_{gM} = \frac{x_1 \Delta C_{p1} T_{g1} + x_3 \Delta C_{P3} T_{g3}}{x_1 \Delta C_{p1} + x_3 \Delta C_{p3}} \quad (A.4)$$

where T_{gi} and ΔC_{Pi} are the glass transition temperature of component *i* and the increment change in heat capacity at $T_{gi.}$, respectively. $x_i=N_i/(N_1+N_3)$ represents the mole fraction of component *i* (N_1 and N_3 are number of absorbed nonsolvent molecules and polymer segments, respectively). The parameters required to estimate T_{gM} and β have been listed in Table A.1.

Insert Table A.1

The calculated values of GRP model for water/PS system at three different temperatures (20, 40 and 60 ℃) have been reported in Table A.2.

Insert Table A.2

5. References

[1] Formhals A. U.S. Patent, 1,975,504, 1934.

[2] Doshi J, Reneker DH. "Electrospinning process and applications of Electrospun fibers", J Electrostat 1995;35(2-3):1698-1703.

[3] Hohman MM, Shin M, Rutledge G, Brenner MP. "Electrospinning and electrically forced jets. I. Stability theory", Phys Fluids 2001;13(8):2201-2220.

[4] Luo CJ, Stoyanov SD, Stride E, Pelan E, Edirisinghe M. "Electrospinning versus fiber production methods: from specifics to technological convergence", Chem Soc Rev 2012;41(13):4708-4735.

[5] Travis JS, Horst A, von Recum HA. "Electrospinning: Applications in drug delivery and tissue engineering", Biomaterials 2008;29(13):1989-2006.

[6] Beachley V, Wen X. "Fabrication of nanofiber reinforced protein structures for tissue engineering", Mater Sci Eng C Mater Biol Appl 2009;29(8):2448-2453.

[7] Huang ZM, Zhang YZ, Kotaki M, Ramakrishna S. "A review on polymer nanofibers by electrospinning and their applications in nanocomposites", Compos Sci Technol 2003;63(15):2223-2253.

[8] Podgorski A, Bałazy A, Gradon L. "Application of nanofibers to improve the filtration efficiency of the most penetrating aerosol particles in fibrous filters", Chem Eng Sci 2006;61(20):6804-6815.

[9] Leung WWF, Hung CH, Yuen PT. "Effect of face velocity, nanofiber packing density and thickness on filtration performance of filters with nanofibers coated on a substrate", Sep Purif Technol 2010;71(1):30-37.

[10] Ramaseshan R, Ramakrishna S. "Zinc Titanate Nanofibers for the Detoxification of Chemical Warfare Simulants", J Am Ceram Soc 2007;90(6):1836–1842.

[11] Miyauchi Y, Ding B, Shiratori S. "Fabrication of a silver-ragwort-leaf-like super-hydrophobic micro/nanoporous fibrous mat surface by electrospinning", Nanotechnology 2006;17(20):5151-5156.

[12] Zheng J, He A, Li J, Xu J, Han CC. "Studies on the controlled morphology and wettability of polystyrene surfaces by electrospinning or electrospraying", Polymer 2006;47(20):7095-7102.

[13] Lin J, Cai Y, Wang X, Ding B, Yu J, Wang M. "Fabrication of biomimetic superhydrophobic surfaces inspired by lotus leaf and silver ragwort leaf", Nanoscale 2011;3(3):1258-1262.

[14] Ding B, Lin J, Wang X, Yu J, Yang J, Cai Y. "Investigation of silica nanoparticle distribution in nanoporous polystyrene fibers", Soft Matter 2011;7(18):8376-8383.

[15] Lin J, Ding B, Yang J, Yu J, Sun G. "Subtle regulation of the micro- and nanostructures of electrospun polystyrene fibers and their application in oil absorption", Nanoscale 2012;4(1):176-182.

[16] Lin J, Shang Y, Ding B, Yang J, Yu J, Al-Deyab SS. "Nanoporous polystyrene fibers for oil spill cleanup", Mar Pollut Bull 2012;64(2):347-352.

[17] Megelski S, Stephens JS, Chase DB, Rabolt JF. "Micro- and nanostructured surface morphology on electrospun polymer fibers", Macromolecules 2002;35(22):8456-8466.

[18] Theron SA, Zussman E, Yarin AL. "Experimental investigation of the governing parameters in the electrospinning of polymer solutions", Polymer 2004;45(6):2017-2030.

[19] Jarusuwannapoom T, Hongrojjanawiwat W, Jitjaicham S, Wannatong L, Nithitanakul M, Pattamaprom C, Koombhongse P, Rangkupan R, Supaphol P. "Effect of solvent on electro-spinnability of polystyrene solutions and morphological appearance of resulting electrospun polystyrene fibers", Eur Polym J 2005;41(3):409-421.

[20] Luo CJ, Nangrejo M, Edirisinghe M. "A novel method of selecting solvents for polymer electrospinning", Polymer 2010;51(7):1654-1662.

[21] Yu JH, Fridrikh SV, Rutledge GC. "The role of elasticity in the formation of electrospun fibers", Polymer 2006;47(13):4789-4797.

[22] Casper CL, Stephens JS, Tassi NG, Chase DB, Rabolt JF. "Controlling surface morphology of electrospun polystyrene fibers: Effect of humidity and molecular weight in the electrospinning process", Macromolecules 2004;37(2): 573-578.

[23] Shenoy SL, Bates WD, Frisch HL, Wnek GE. "Role of chain entanglements on fiber formation during electrospinning of polymer solutions: good solvents, non-specific polymer-polymer interaction limit", Polymer 2005;46(10):3372-3384.

[24] Pai CL, Boyce MC, Rutledge GC. "Morphology of porous and wrinkled fibers of polystyrene electrospun from Dimethylformamide", Macromolecules 2009;42(6):2102-2114.

[25] Vrieze SD, Camp TV, Nelvig A, Hagstrom B, Westbroek P, Clerck KD. "The effect of temperature and humidity on electrospinning", J Mater Sci 2009;44(5):1357-1362.

[26] Kim GT, Lee JS, Shin JH, Ahn YC, Hwang YJ, Shin HS, Lee JK, Sung CM. "Investigation of pore formation for polystyrene electrospun fibers", Korean J Chem Eng 2005;22(5):783-788.

[27] Park JY, Lee IH. "Relative humidity effect on the preparation of porous electrospun polystyrene fibers", J. Nanosci Nanotechnol 2010;10(5): 3473-3477.

[28] Tripatanasuwan S, Zhong Z, Reneker DH. "Effect of evaporation and solidification of the charged jet in electrospinning of poly(ethylene oxide) aqueous solution", Polymer 2007;48(19):5742-5746.

[29] Patel AC, Li Sh, Wang Ce, Zhang W, Wei Y. "Electrospinning of Porous Silica Nanofibers Containing Silver Nanoparticles for Catalytic Applications", Chem Mater 2007;19(6):1231–1238.

[30] Zhang Y, Li J, An G, He X. "Highly porous SnO2 fibers by electrospinning and oxygen plasma etching and its ethanol-sensing properties", Sensor Actuat B-Chem 2010;144(1):43-48.

[31] Bognitzki M, Czado W, Frese T, Schaper A, Hellwig M, Steinhart M, Greiner A, Wendorff JH. "Nanostructured fibers via electrospinning", Adv Mater 2001;13(1):70-72.

[32] Han SO, Son WK, Youk JH, Lee TS, Park WH. "Ultrafine porous fibers electrospun from cellulose triacetate", Mater Lett 2005;59(24-25):2998-3001.

[33] Zhang YZ, Feng Y, Huang M, Ramakrishna S, Lim CT. "Fabrication of porous electrospun nanofibers", Nanotechnology 2006;17(3):901-908.

[34] McCann JT, Marquez M, Xia Y. "Highly porous fibers by electrospinning into a cryogenic liquid", J Am Chem Soc 2006;128(5):1436-1437.

[35] Gupta A, Saquing CD, Afshari M, Tonelli AE, Khan SA, Kotek R. "Porous Nylon-6 fibers via a novel salt-induced electrospinning method", Macromolecules 2009;42(3):709-715.

[36] Dayal P, Kyu T. "Porous fiber formation in polymer-solvent system undergoing solvent evaporation", J Appl Phys 2006;100(4):1-6.

[37] Dayal P, Liu J, Kumar S, Kyu T. "Experimental and theoretical investigation of porous structure formation in electrospun fibers", Macromolecules 2007;40(21):7689-7694.

[38] Dayal P, Kyu T. "Dynamics and morphology development in electrospun fibers driven by concentration sweep", Phys Fluids 2007;19(10):1-9.

[39] Qi Z, Yu H, Chen Y, Zhu M. "Highly porous fibers prepared by electrospinning a ternary system of nonsolvent/solvent/poly($_L$-lactic acid)", Mater Lett 2009;63(3-4):415-418.

[40] Lin J, Ding B, Yu J, Hsieh Y. "Direct fabrication of highly nanoporous polystyrene fibers via electrospinning", Appl Mater Interfaces 2010;2(2):521-528

[41] Demir MM. "Investigation on glassy skin formation of porous polystyrene fibers electrospun from DMF", eXPRESS Polym Lett 2010;4(1):2-8.

[42] Celebioglu A, Uyar T. "Electrospun porous cellulose acetate fibers from volatile solvent mixture", Mater Lett 2011;65(14):2291-2294.

[43] Nayani K, Katepalli H, Sharma CS, Sharma A, Patil S, Venkataraghavan R. "Electrospinning combined with nonsolvent-induced phase separation to fabricate highly porous and hollow submicrometer polymer fibers", Ind Eng Chem Res 2012;51(4):1761–1766.

[44] Huang L, Bui NN, Manickam SS, McCutcheon JR. "Controlling electrospun nanofiber morphology and mechanical properties using humidity", J Polym Sci Pol Phys 2011;49(24):1734-1744.

[45] Yu X, Xiang H, Long Y, Zhao N, Zhang X, Xu J. "Preparation of porous polyacrylonitrile fibers by electrospinning a ternary system of PAN/DMF/H_2O", Mater Lett 2010;64(22):2407-2409.

[46] Seo YA, Pant HR, Nirmala R, Lee JH, Song KG, Kim HY. "Fabrication of highly porous poly(ε-caprolactone) microfibers via electrospinning", J Porous Mat 2012;19(2):217-223.

[47] Zheng J, Zhang H, Zhao Z, Han CC. "Construction of hierarchical structures by electrospinning or electrospraying", Polymer 2012;53(2):546-554.

[48] Sonntag RE, Borgnakke C, van Wylen GJ. Fundamentals of thermodynamics, 6th Edition. United States of America: John Wiley & Sons Inc, 2003.

[49] Tompa H. Polymer Solution. London: Butterworth, 1956.

[50] Yilmaz L, McHugh AJ. "Analysis of nonsolvent-solvent-polymer phase diagrams and their relevance to membrane formation modeling", J Appl Polym Sci 1986;31():997-1018.

[51] Altena FW, Smolders CA. "Calculations of liqyuid-liquid phase separation in a ternary system of a polymer in a mixture of solvent and a nonsolvent" Macromolecules 1982;15(6):1491-1497.

[52] Karimi M, Albrecht W, Heuchel M, Kish MH, Frahn J, Weigel Th, Hofmann D, Modarress H, Lendlein A. "Determination of water/polymer interaction parameter for membrane-forming systems by sorption measurement and a fitting technique", J Membrane Sci 2005;265(1-2):1-12.

[53] Karimi M, Albrecht W, Heuchel M, Weigel Th, Lendlein A. "Determination of solvent/polymer interaction parameters of moderately concentrated polymer solutions by vapor pressure osmometry", Polymer 2008;49(10):2587-2594.

[54] Karimi M, Heuchel M, Albrecht W, Hofmann D. "A lattice-fluid model for the determination of the water/polymer interaction parameter from water uptake measurements", J Membrane Sci 2007;292(1-2):80-91.

[55] Tan L, Pan D, Pan N. "Thermodynamic Study of a Water–Dimethylformamide–Polyacrylonitrile Ternary System", J Appl Polym Sci 2008;110(6):3439–3447.

[56] Barth C, Horst R, Wolf BA. "(Vapour+liquid) equilibria of (water+dimethylformamide): application of the headspace-gas chromatography for the determination of thermodynamic interactions", J Chem Thermodyn 1998;30(5):641-652.

[57] Reuvers AJ. "Membrane formation (diffusion-induced demixing processes in ternary polymeric systems) ", PhD Thesis, University of Twente, Enschede, The Netherlands, 1987.

[58] Wolf BA, Willms MM. "Measured and calculated solubility of polymers in mixed solvents: Co-nonsolvency", Makromol Chem Phys 1978;179(9):2265–2277.

[59] Shiomi T, Kuroki K, Kobayashi A, Nikaido H, Yokoyama M, Tezuka Y, Imai K. "Dependence of swelling degree on solvent composition of two-component copolymer networks in mixed solvents", Polymer 1995;36(12):2443- 2449.

[60] Nunes SP, Inoue T. "Evidence for spinodal decomposition and nucleation and growth mechanism during membrane formation", J Membrane Sci 1996;111(1):93-103.

[61] Pauchard L, Allain C. "Buckling instability induced by polymer solution drying", Europhys Lett 2003;62(6):897-903.

[62] Pauchard L, Hulin JP, Allain C. "Drops that buckle" Europhys News 2005; 36(1):9-11.

[63] Vrentas JS. "Diffusion in polymer-solvent systems. II. A predictive theory for the dependence of diffusion coefficients on temperature, concentration and molecular weight", J Polym Sci Pol Phys 1977;15(3):417-439.

[64] Tsai JT, Su YS, Wang DM, Kuo JL, Lai JY, Deratani A, "Retainment of pore connectivity in membranes prepared with vapor-induced phase separation", J Membrane Sci 2010;362(1-2):360-373.

[65] Park MS, Kim JK. "Breath figure patterns prepared by spin coating in a dry environment", Langmuir 2004;20(13):5347-5352.

[66] Francois B, Pitois O, Francois J. "Polymer films with a self-organized honeycomb morphology", Adv Mater 1995;7(12):1041-1044.

[67] Peng J, Han Y, Yang Y, Li B. "The influencing factors on the macroporous formation in polymer films by water droplet templating", Polymer 2004;45(2):447-452, 2004.

[68] Limaye AV, Narhe RD, Dhote AM, Ogale SB. "Evidence for convective effects in breath figure formation on volatile fluid surface", Phys Rev Lett 1996;76(20):3762-3765.

[69] Srinivasarao M, Collings D, Philips A, Patel S. "Three-dimensionally ordered array of air bubbles in a polymer film", Science 2001;292(5514):79-83.

[70] Eda G, Shivkumar S. "Bead-to-Fiber Transition in Electrospun Polystyrene", J Appl Polym Sci 2007;106(1):475-487.

[71] Luo CJ, Stride E, Edirisinghe M. "Mapping the influence of solubility and dielectric constant on electrospinning polycaprolactone solutions", Macromolecules 2012;45(11): 4669-4680.

[72] Ruzette AVG, Mayes AM. "A Simple Free Energy Model for Weakly Interacting Polymer Blends", Macromolecules 2001;34(6):1894-1907.

[73] Wunderlich B. Thermal analysis of polymeric materials. New York: Springer, Berlin Heidelberg, 2005.

[74] Johari GP, Hallbrucker A, Mayer E. "The glass-liquid transition of hyperquenched water", Nature 1987;330:552-553.

Table 1. Required parameters to calculate ternary phase diagram of H_2O/DMF/PS and H_2O/THF/PS systems

T (ºC)	$\chi_{H_2O/DMF}$ [55, 56]			$\chi_{H_2O/THF}$ [a]			$\chi_{H_2O/PS}$	$\chi_{DMF/PS}$	$\chi_{THF/PS}$
	α_0	β_0	γ_0	α_0	β_0	γ_0			
20	0.218	0.276	-0.622	0.720	0.764	0.531	3.1	0.499	0.470
40	0.4250	0.0619	0.9494	0.724	0.781	0.546	2.5		
60	0.1511	0.1553	0.8751	0.724	0.820	0.546	2.3		

[a] Calculated according to UNIFAC method

Table 2. Mean value of surface pore diameter of fibers electrospun from 20 wt.% PS/DMF solution at various environmental conditions

Temperature (℃)	Mean pore diameter (nm)			
	RH: 30%	RH: 40%	RH: 50%	RH: 60%
20	64.06	66.477	78.35	92.06
40	43.46	70.87	113.26	147.27
60	-------	133.84	79.34	124.42

Table A.1. Required parameters to calculate Water/PS interaction parameter

Polystyrene (PS)				Water	
$T_{g3}(K)$	$\Delta C_{P3}(T_{g3})$ ($J\ mol^{-1}\ K^{-1}$)	$\rho^{*}\ (g/cm^{3})$	$\alpha(1/K)$	$T_{g1}(K)$	$\Delta C_{P1}(T_{g1})$ ($J\ mol^{-1}\ K^{-1}$)
373[a]	30.8 [73]	1.24 [72]	5.13×10^{-4} [72]	138 [74]	34.9 [74]

[a]: measured by Differential Scanning Calorimetry (DSC)

Table A.2. Calculated values of GRP model for Water/PS system at three different temperatures

Temperature (℃)	Water uptake $mg_{water}/mg_{polymer}$	T_{gM} (K)	β	$\rho(T)$	φ_{FV}
20	0.006	364.25	0.11	1.067	0.1396
40	0.019	350.82	0.37	1.056	0.1484
60	0.046	318.06	1	1.045	0.1571

Figure Captions

Figure 1. Schematic representation of electrospinning chamber

Figure 2. Variation of absolute humidity with temperature as a function of relative humidity. Open circles denote to environmental conditions under which electrospinning has been performed

Figure 3. Theoretical binodal curve and experimentally calculated cloud points for (a) H_2O/DMF/PS and (b) H_2O/THF/PS systems at three temperatures (20, 40 and 60 ℃)

Figure 4. Variation of g_{12} with water content for Water/THF and Water/DMF at different temperatures

Figure 5. Schematic representation of three possible composition paths which fibers undergo during electrospinning process

Figure 6. Cross-sectional SEM image of fibers electrospun from 20 wt.% PS/DMF solutions at 20 ℃ and different levels of R elative Humidity (RH): (a) 20%, (b) 30%, (c) 40%, (d) 50%, (e) 60%.

Figure 7. Cross-sectional SEM image of fibers electrospun from 20 wt.% PS/DMF solutions at 40 ℃ and different levels of R elative Humidity (RH): (a) 20%, (b) 30%, (c) 40%, (d) 50%, (e) 60%.

Figure 8. Cross-sectional SEM image of fibers electrospun from PS/DMF solutions at 60 ℃ and different levels of RH: (a) 10% (two stuck fibers), (b) 20%, (c) 30%, (d) 40%, (e) 50%, (f) 60%.

Figure 9. Fractional interior pore volume (FPV) of fibers produced from 20 wt.% PS/DMF solutions at different environmental conditions

Figure 10. Cross-sectional SEM image of fibers electrospun from 20 wt.% PS/THF solutions at different environmental conditions: (a) 20 ℃-20%RH, (b) 20 ℃-60%RH, (c) 40 ℃-20%RH, (d) 40 ℃- 60%RH.

Figure 11. Cross-sectional SEM image of fibers electrospun at 40 ℃ and 60% RH from 20 wt.% PS/(THF:DMF) solutions with different THF:DMF ratios: (a) 100:0, (b) 70:30, (c) 60:40, (d) 50:50, (e) 0:100.

Figure 12. Variation of fractional interior pore volume (FPV) of fibers electrospun from PS/(THF:DMF) with solvent composition

Figure 13. Surface morphology of electrospun fibers from 20 wt.% PS/DMF solutions at different environmental conditions

Figure 14. Schematic representation of regions in which electrospun PS/DMF fibers with specific surface and interior morphology can be observed

Figure 1

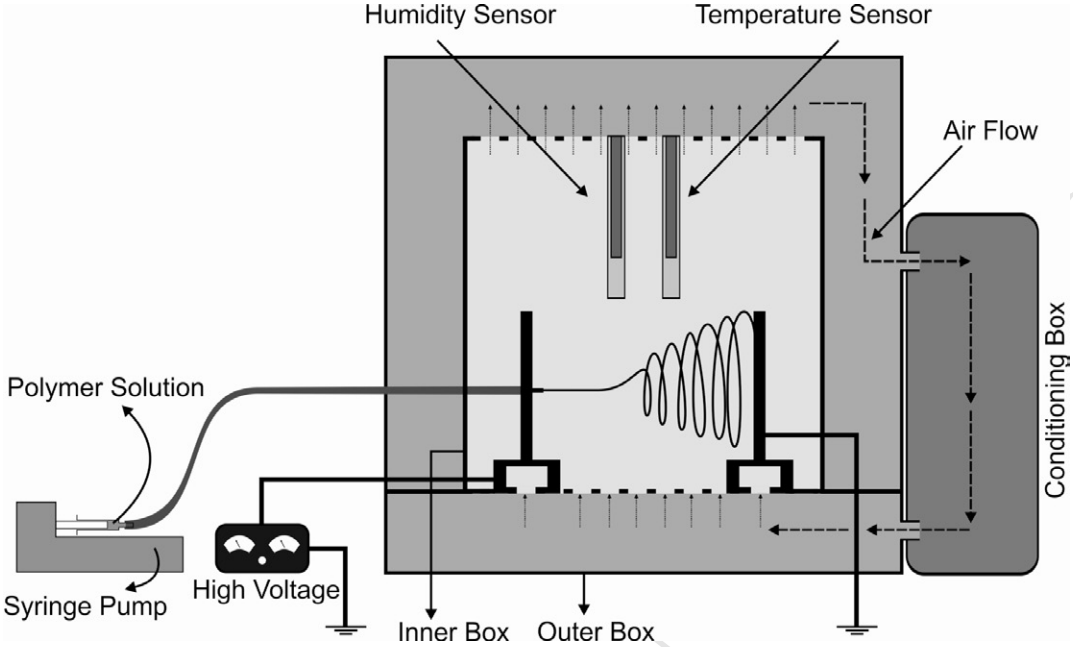

Figure 2

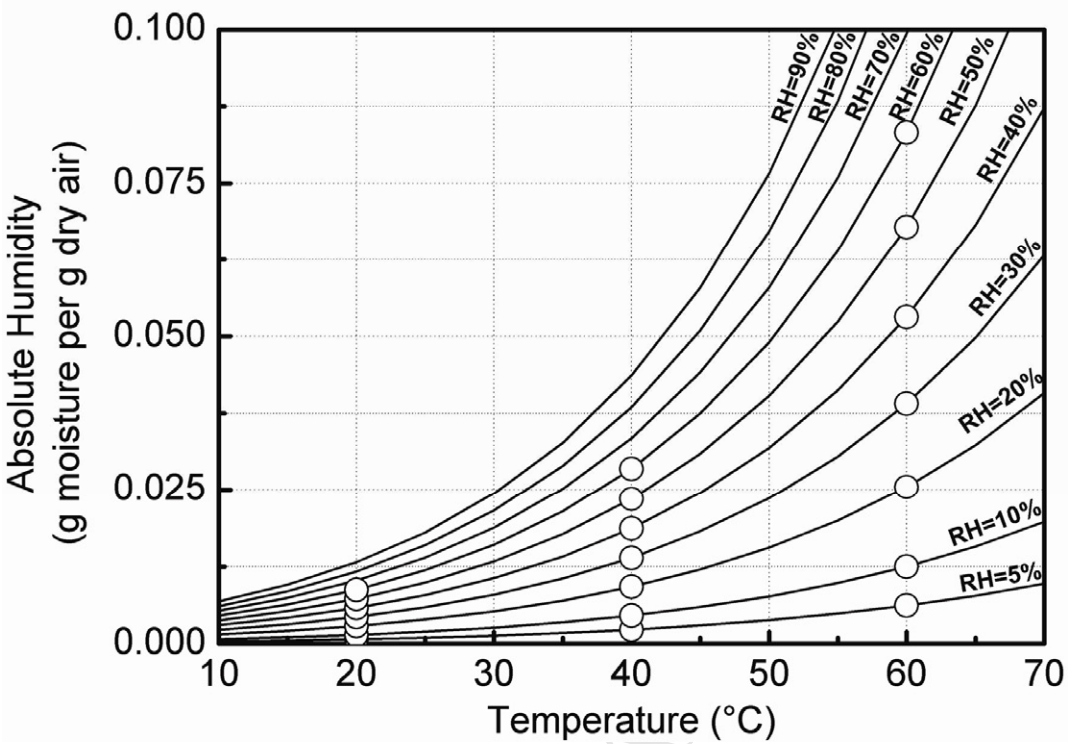

Figure 3

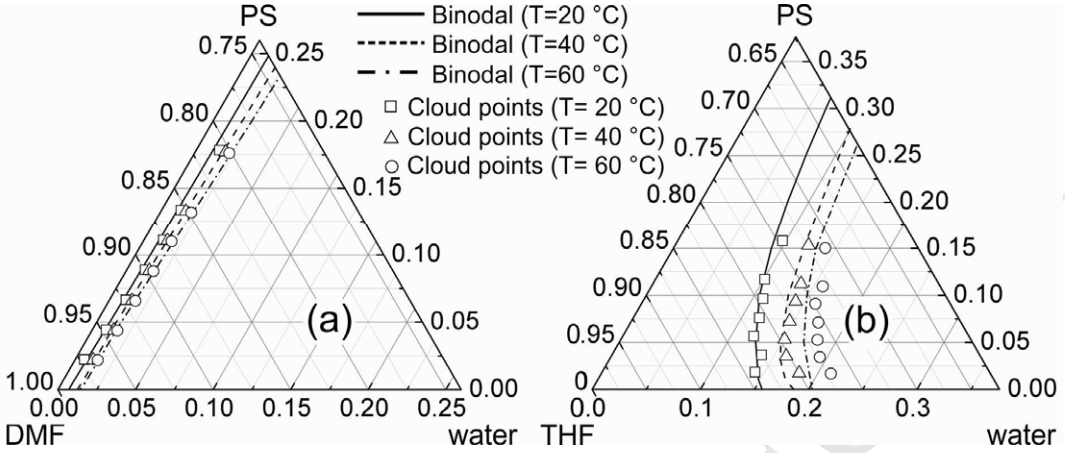
PS
Binodal (T=20 °C)
Binodal (T=40 °C)
Binodal (T=60 °C)
Cloud points (T= 20 °C)
Cloud points (T= 40 °C)
Cloud points (T= 60 °C)
0.75
0.80
0.85
0.90
0.95
1.00
0.25
0.20
0.15
0.10
0.05
0.00
(a)
0.00 0.05 0.10 0.15 0.20 0.25
DMF
water
PS
0.65
0.70
0.75
0.80
0.85
0.90
0.95
0
0.35
0.30
0.25
0.20
0.15
0.10
0.05
0.00
(b)
0.0 0.1 0.2 0.3
THF
water

Figure 4

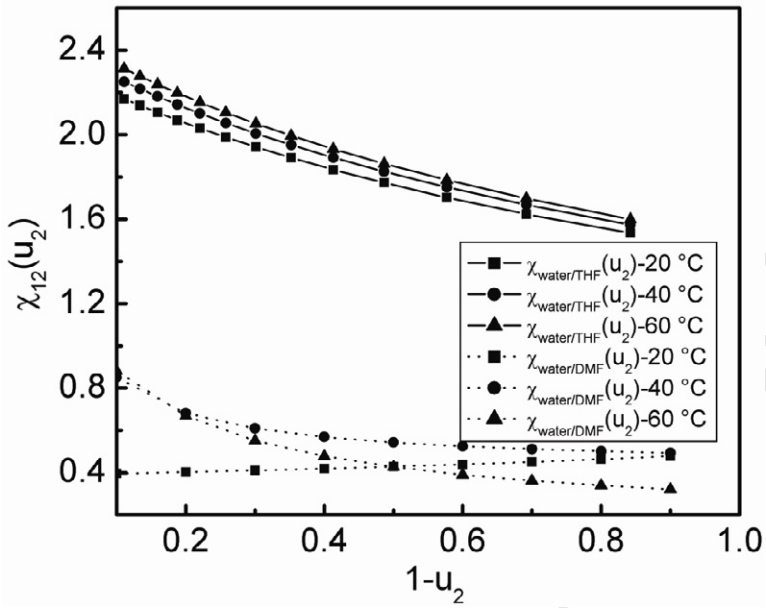

Figure 5

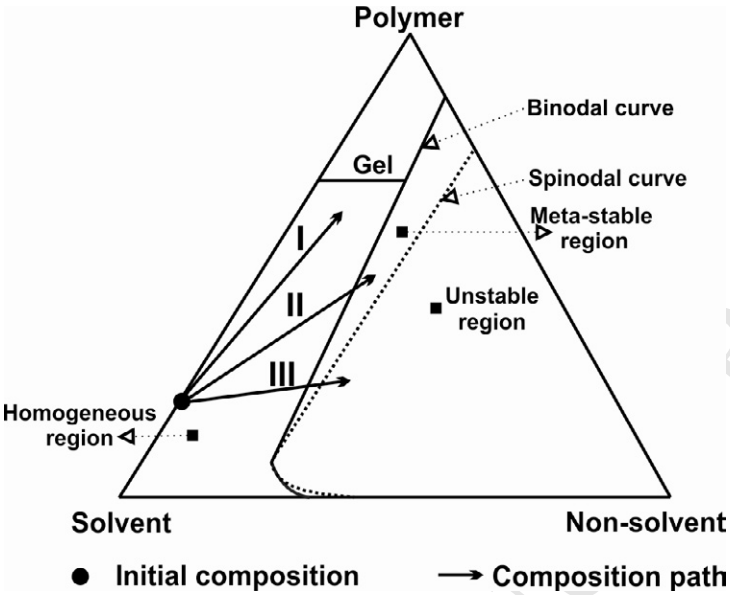

Figure 6

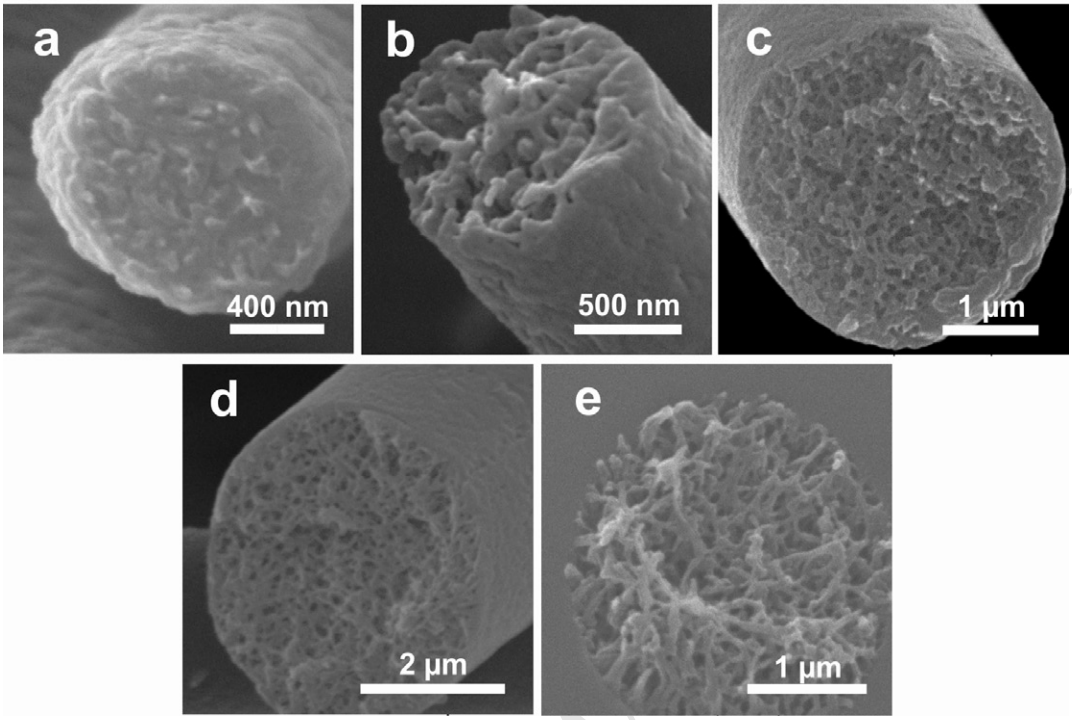

Figure 7

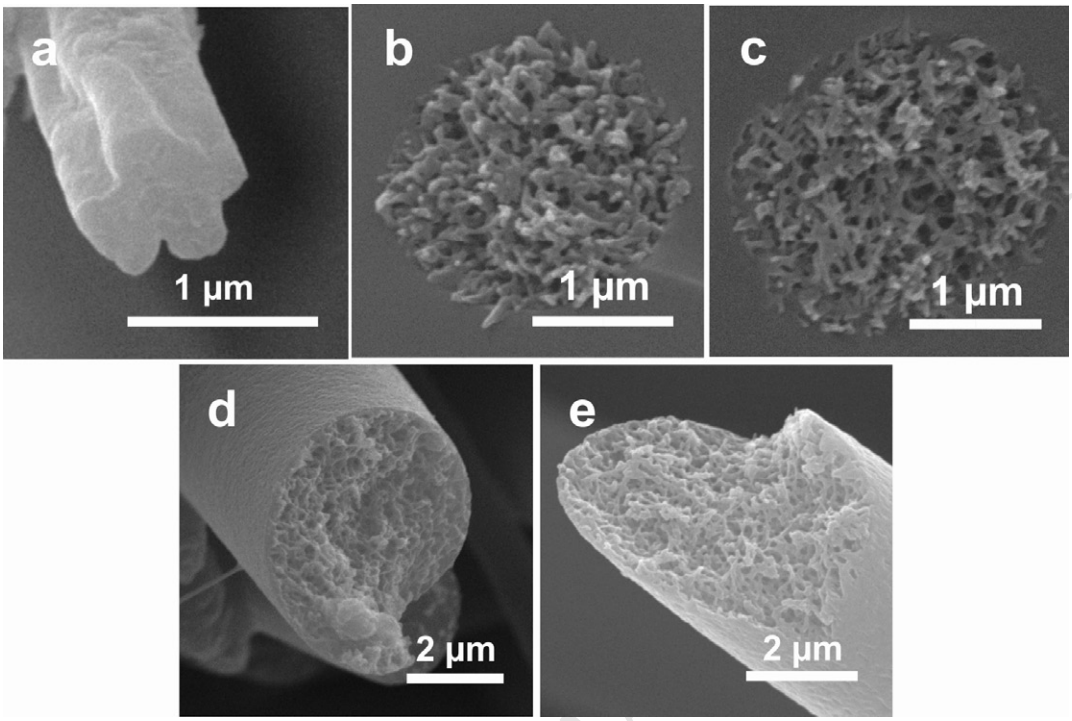

Figure 8

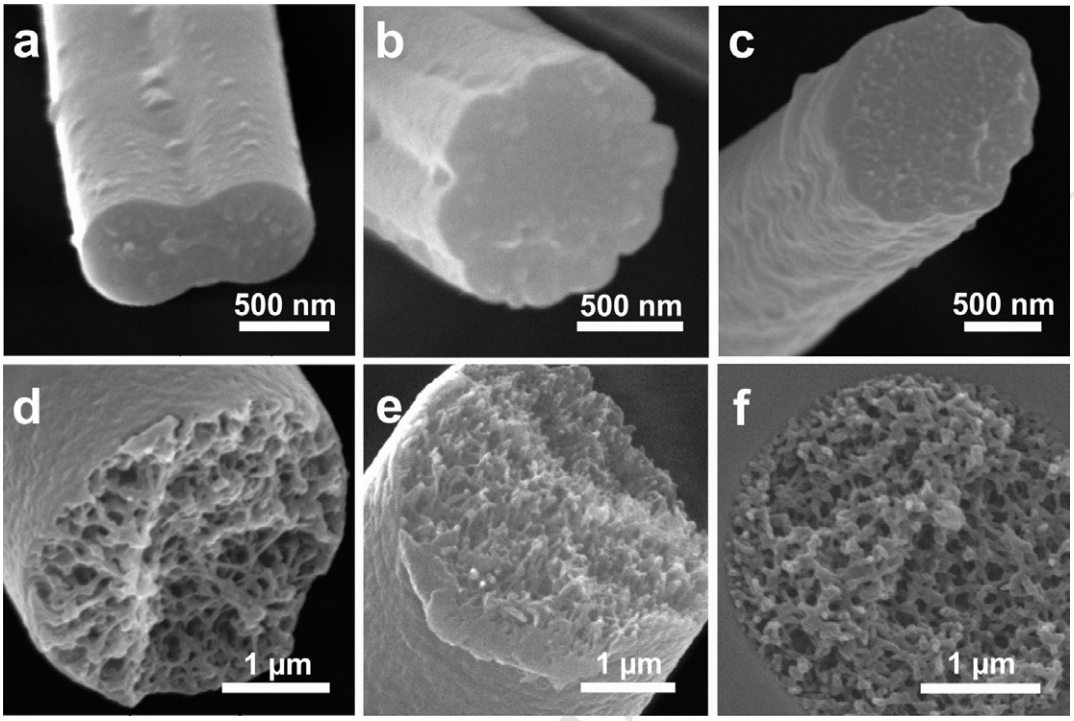

Figure 9

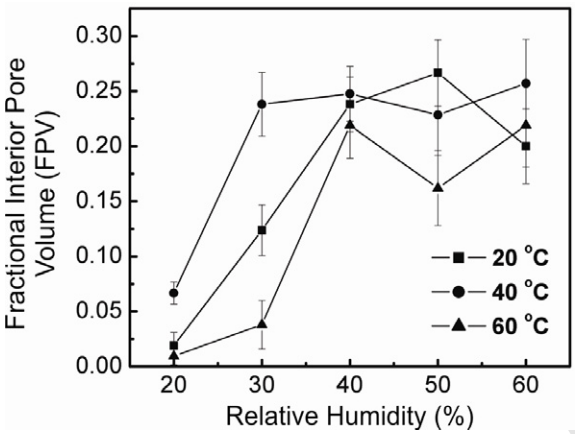

Figure 10

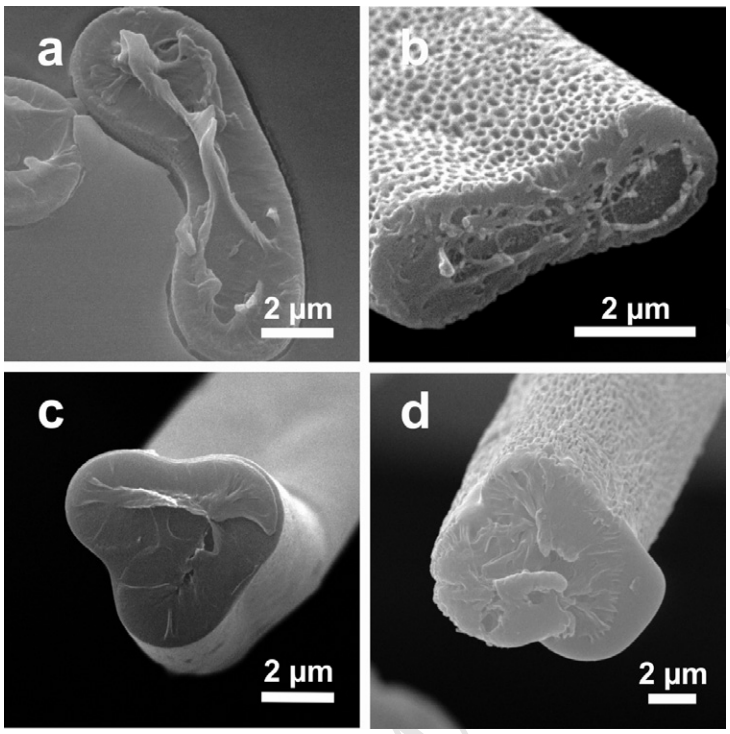

Figure 11

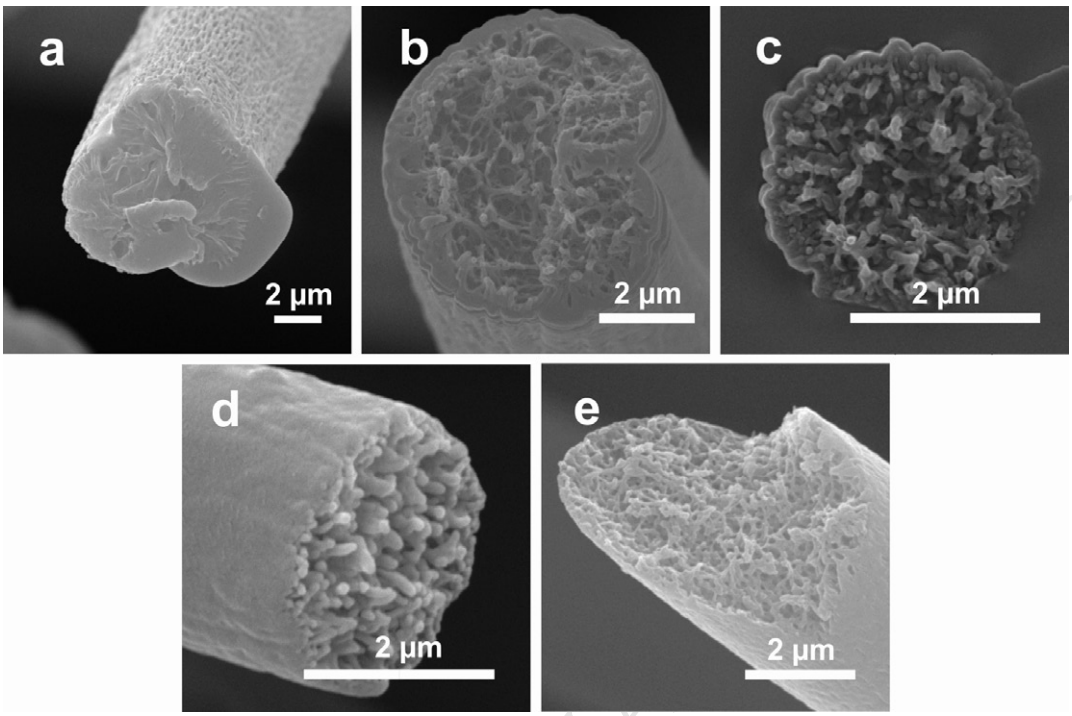

Figure 12

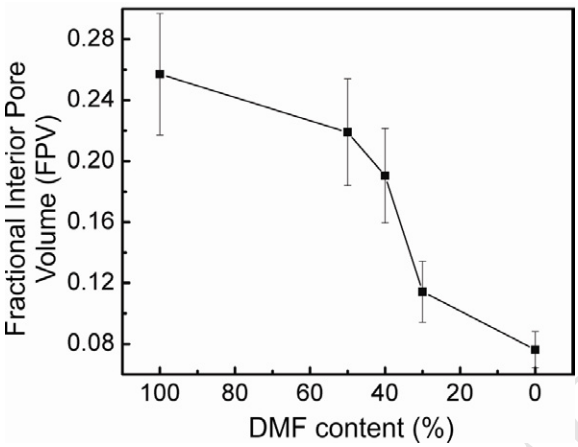

Figure 13

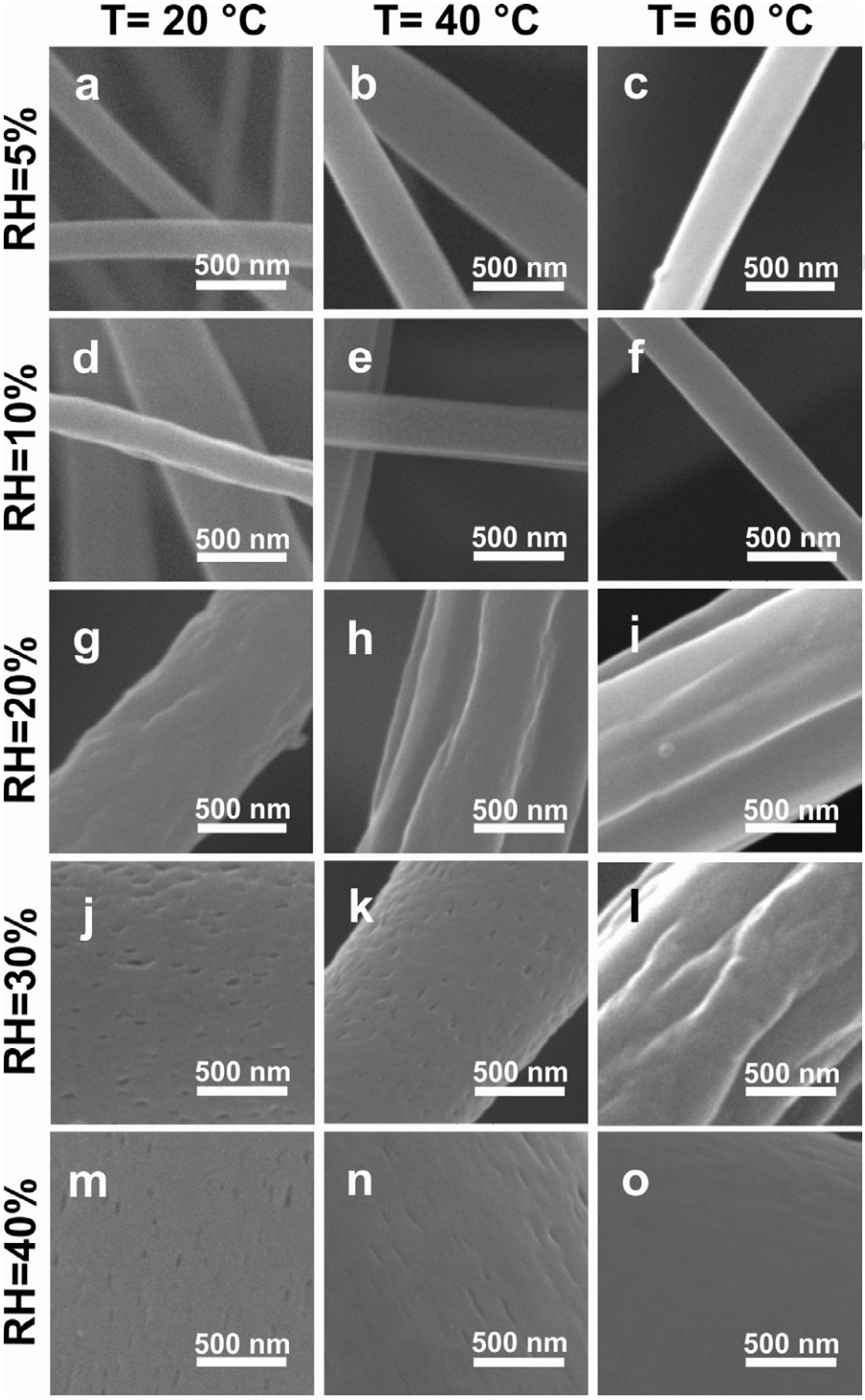
T= 20 °C
T= 40 °C
T= 60 °C
RH=5%
RH=10%
RH=20%
RH=30%
RH=40%
a
b
c
d
e
f
g
h
i
j
k
l
m
n
o
500 nm

Figure 13 (Continued)

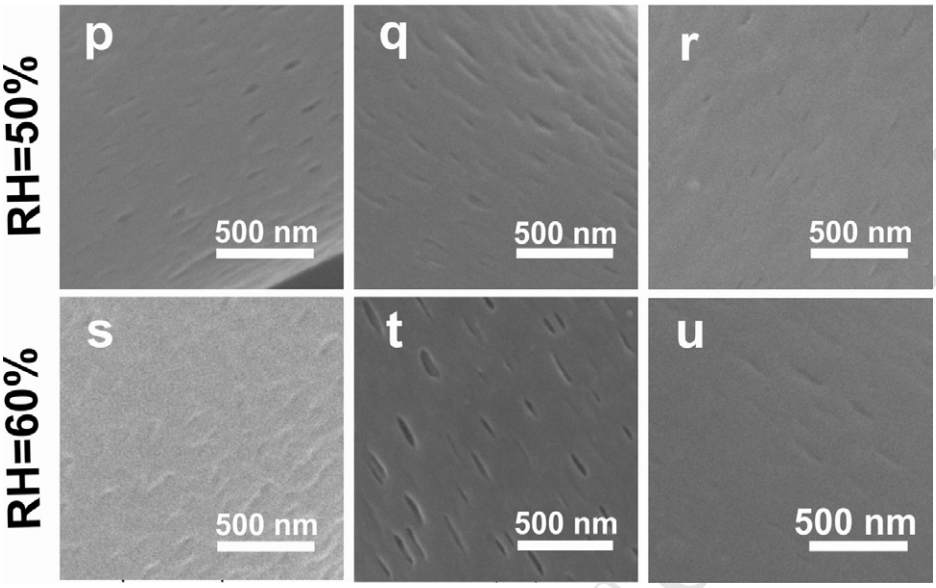

Figure 14

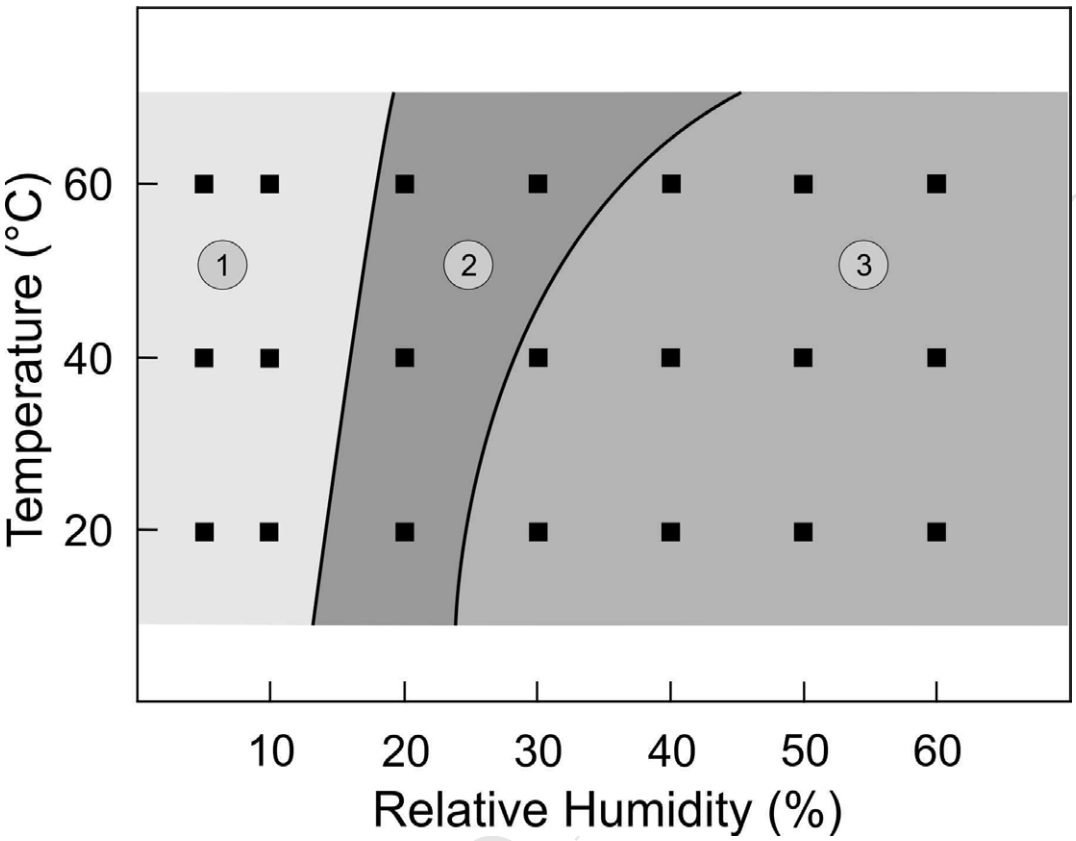

Figure 15

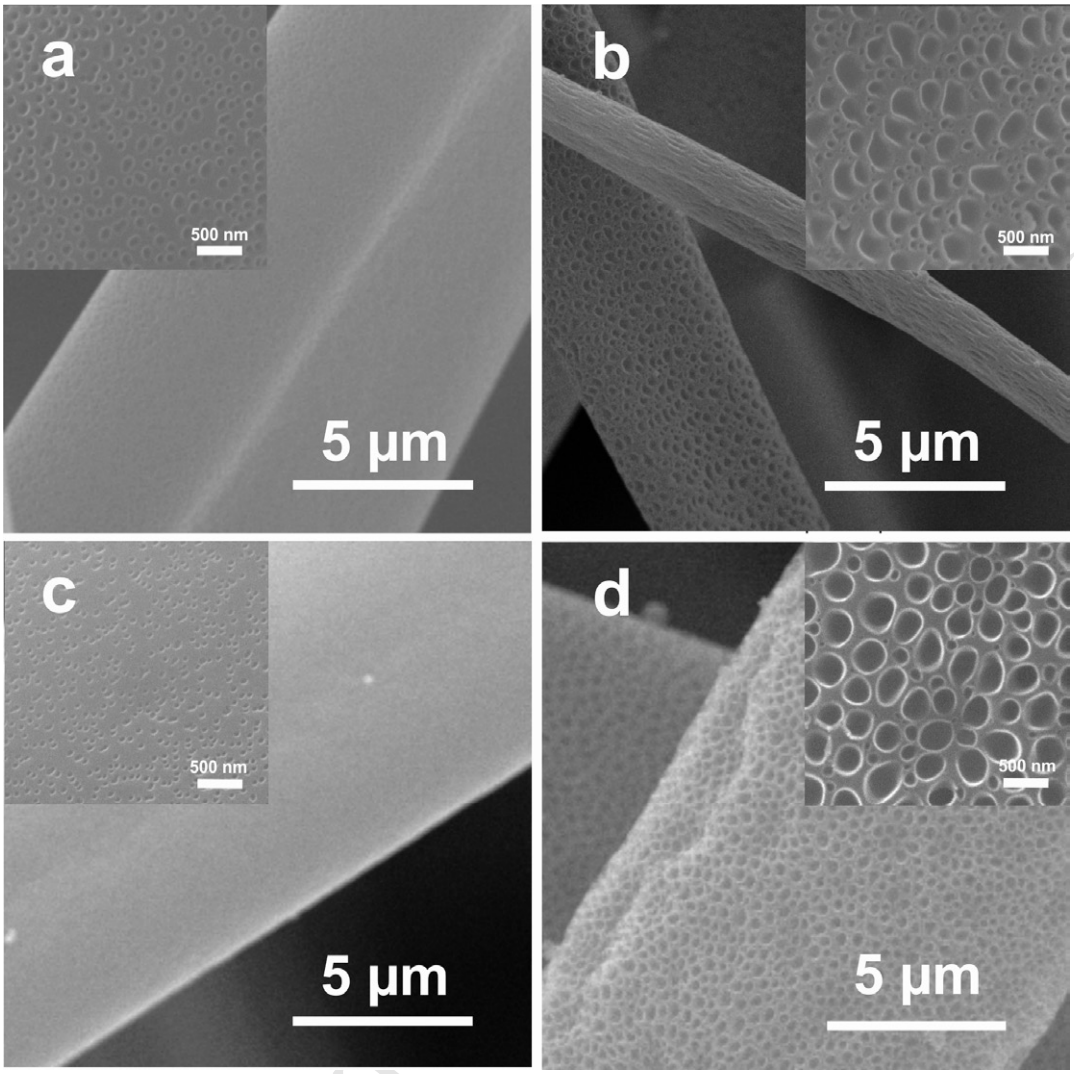

Figure 16

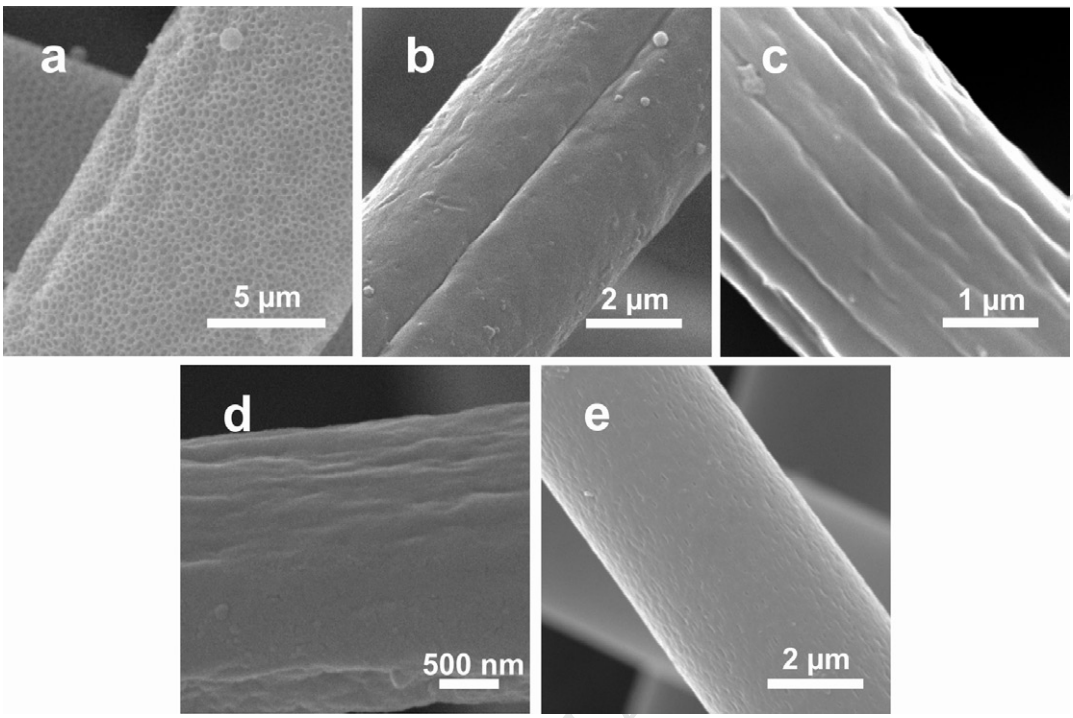

Figure 17

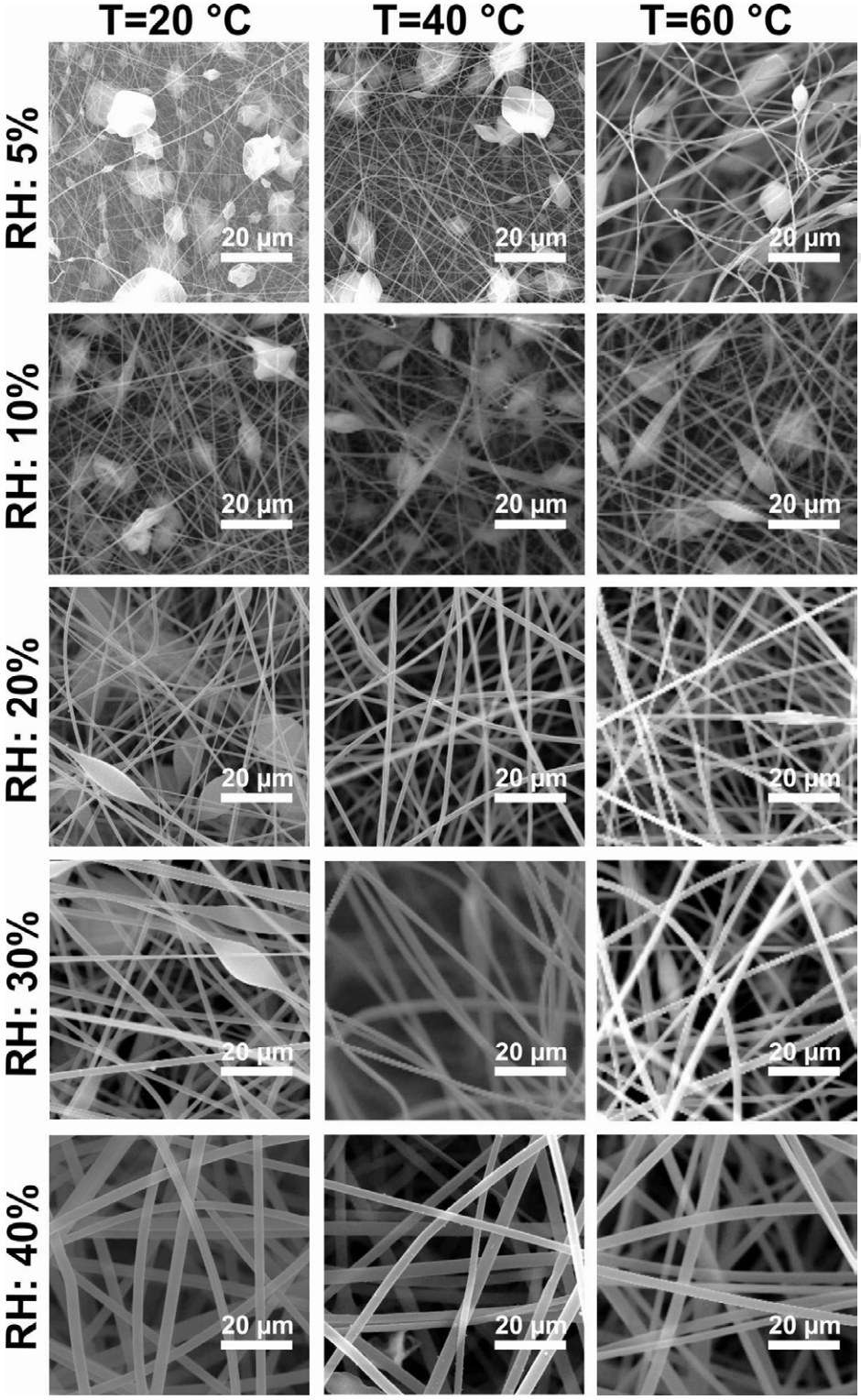

Figure 17 (Continued)

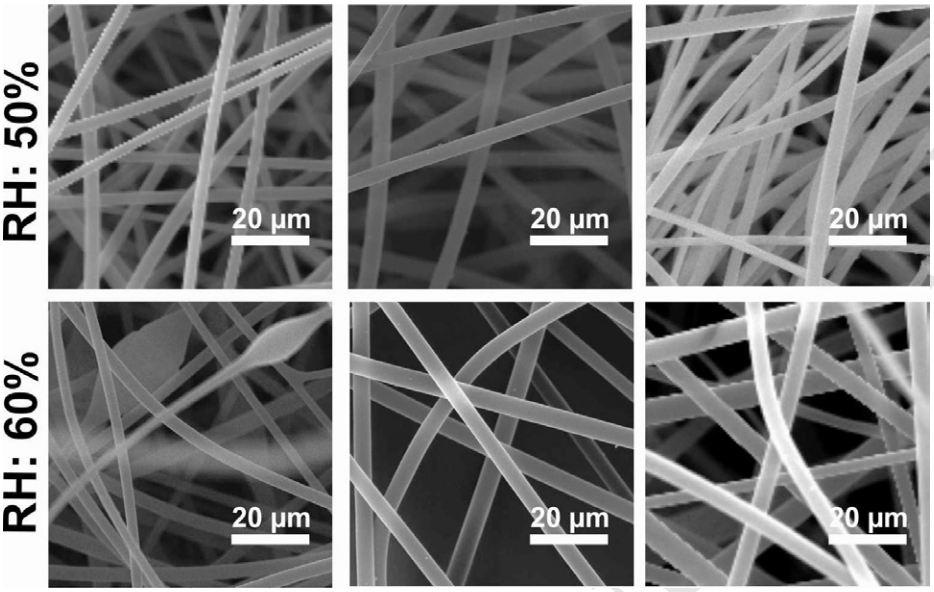

Figure 18